
Article:
Yusuf, L., Heatley, M.C., Palmer, J.P.G. et al. (3 more authors) (2020) Noncoding regions underpin avian bill shape diversification at macroevolutionary scales. Genome Research, 30 (4). pp. 553-565. ISSN 1088-9051

https://doi.org/10.1101/gr.255752.119

Noncoding regions underpin avian bill shape diversification at macroevolutionary scales

Leeban Yusuf[1,2], Matthew C. Heatley[1,3], Joseph P.G. Palmer[1,4], Henry J. Barton[1,5], Christopher R. Cooney[1,*], Toni I. Gossmann[1,6,*]

[1] Department of Animal and Plant Sciences, University of Sheffield, Sheffield S10 2TN, UK

[2] Centre for Biological Diversity, School of Biology, University of St. Andrews, Fife, KY16 9TF, UK

[3] Division of Plant and Crop Sciences, School of Biosciences, University of Nottingham, Sutton Bonington LE12 5RD, UK

[4] School of Biological Sciences, Royal Holloway University of London, Egham, Surrey, TW20 0EX, UK

[5] Organismal and Evolutionary Biology Research Programme, Viikinkaari 9 (PL 56), University of Helsinki, Helsinki, FI-00014, Finland

[6] Department of Animal Behaviour, Bielefeld University, Postfach 100131, Bielefeld, DE-33501, Germany

[*] **Correspondance:** c.cooney@sheffield.ac.uk (CRC) and toni.gossmann@gmail.com (TIG)

Keywords: Comparative genomics, BMP and Wnt signalling, bird beak shape morphology, regulatory changes, avian-specific highly conserved elements

Abstract

Recent progress has been made in identifying genomic regions implicated in trait evolution on a microevolutionary scale in many species, but whether these are relevant over macroevolutionary time remains unclear. Here, we directly address this fundamental question using bird beak shape, a key evolutionary innovation linked to patterns of resource use, divergence and speciation, as a model trait. We integrate class-wide geometric-morphometric analyses with evolutionary sequence analyses of 10,322 protein coding genes as well as 229,001 genomic regions spanning 72 species. We identify 1,434 protein coding genes and 39,806 noncoding regions for which molecular rates were significantly related to rates of bill shape evolution. We show that homologs of the identified protein coding genes as well as genes in close proximity to the identified noncoding regions are involved in craniofacial embryo development in mammals. They are associated with embryonic stem cells pathways, including BMP and Wnt signalling, both of which have repeatedly been implicated in the morphological development of avian beaks. This suggests that identifying genotype-phenotype association on a genome wide scale over macroevolutionary time is feasible. While the coding and noncoding gene sets are associated with similar pathways, the actual genes are highly distinct, with significantly reduced overlap between them and bill-related phenotype associations specific to noncoding loci. Evidence for signatures of recent diversifying selection on our identified noncoding loci in Darwin finch populations further suggests that regulatory rather than coding changes are major drivers of morphological diversification over macroevolutionary times.

Introduction

Disentangling the interplay between macroevolutionary trends and microevolutionary processes is fundamental to understand patterns of diversification over time. Key innovations, defined as traits that allow species to interact with environments in novel ways (Stroud and Losos 2016), are thought to play an important role determining macroevolutionary patterns of diversification, by allowing lineages to access and exploit new, previously inaccessible resources (Hunter 1998). In birds, evolutionary transitions in life-history traits and the emergence of *de-novo* innovations occurred rapidly alongside species and niche diversification (Balanoff et al. 2013; Xu et al. 2014). Understanding whether convergent molecular mechanisms underlie independent trait evolution in different organisms is a key question in biology (Manceau et al. 2010; Rosenblum et al. 2014; Lamichhaney et al. 2019). A variety of approaches to link molecular and phenotypic changes have been developed (O'Connor and Mundy 2009, 2013; Mayrose and Otto 2011; Levy Karin et al. 2017; Sharma et al. 2018; Hu et al. 2019) but these are generally restricted to relatively simple discretized phenotypic information (Prudent et al. 2016) and may not be easily applicable to more complex phenotypes on a genome-wide scale (Lartillot 2013).

A pertinent example of an important innovation is the evolution of the beak in modern birds. The avian bill is closely associated with species' dietary and foraging niches and changes in beak shape are implicated in driving population divergence and speciation (Grant and Grant 1996; Bhullar et al. 2016). However, despite considerable effort, the genetic and developmental underpinnings of avian beak shape is still poorly understood, particularly at macroevolutionary scales. In the wake of the Cretaceous-Paleogene (K-Pg) mass extinction event, beak shape has been hypothesized to have evolved through a series of ontogenic stages (Bhullar et al. 2012, 2015), though the exact mechanism is yet to be established. Beak shape is comprised of separate morphological and developmental parameters, each of which is likely to be regulated by independent sets of transcriptional factors (Bhullar et al. 2015; Mallarino et al. 2011). Understanding how each of these morphological parameters evolved, how they are modulated, and how changes in such factors affect patterns of beak shape disparity across modern birds represents a significant unresolved challenge.

Several candidate genes linked to bird beak shape have been identified within populations or between recently diverged species. Among the earliest studies to identify genes implicated in beak shape evo-

lution are comparative transcriptomic analyses in Darwin's finches (Abzhanov et al. 2004, 2006) that found *BMP4*, a gene involved in the regulation of beak depth and width, and *CAM* (calmodulin), a gene putatively involved in beak length. Both genes were later identified to be partially-implicated in beak shape development (Mallarino et al. 2011). In addition, *ALX1*, a transcription factor involved in craniofacial development, and *HMGA2*, a gene associated with increases in beak size, were also identified in Darwin's finches (Lamichhaney et al. 2015, 2018). In European populations of great tits, a collagen gene, *COL4A5*, putatively linked to beak length variation, was found to be under selection (Bosse et al. 2017a). Collectively, these findings illustrate (I) a complex genetic architecture for beak shape, (II) that genes implicated in beak shape may evolve under strong, detectable selective pressures in populations, and (III) that such genes are likely to be different across different avian taxonomic groups.

However, despite these clear predictions, no previous attempts have been made to identify genes that repeatedly play a role in beak shape evolution over broad evolutionary timescales. While previous studies have explored the genetic basis of other key avian traits (e.g. song, flight), such studies are typically targeted towards candidate genes, or incorporated clade-specific features (Whitney et al. 2014; Wirthlin et al. 2014; Machado et al. 2016; Sackton et al. 2019). Thus, relatively little is currently known about the genetics underpinning the macroevolution of beak shape. The current lack of insight connecting species or clade specific candidate genes to large scale evolutionary time may be explained by two main arguments. First, there is a growing consensus that large-effect genes (Fisher 1930) may not be as important for the evolution of complex traits as small-effect genes (Hill 2010; Rockman 2012; Boyle et al. 2017). This model of adaptation is well-supported by growing population genomic evidence, but does not explain candidate genes implicated in beak shape evolution with seemingly large-effects on beak morphology and speciation. Second, genes under strong long-term selective pressures may simply be difficult to detect due to confounding factors that obscure evolutionary signals. For example, selective pressures and demography vary over time, making the detection of clear signals of adaptive evolution and other evolutionary forces using sequence divergence approaches challenging. A third possibility is that the role of convergent evolution (Stern 2013; Manceau et al. 2010; Rosenblum et al. 2014; Lamichhaney et al. 2019) is limited if different genes are involved in morphological changes in different parts of the phylogeny.

Here, we utilize large-scale comparative genomic and phylogenetically reconstructed geometric-

morphometric data to identify candidate loci that relate to macroevolutionary shifts in trait evolution. Specifically, we ask whether rates of bird beak shape evolution are explained by loci that experience long-term, repeated shifts in molecular rates across distantly-related avian taxa. To accomplish this, we designed an approach to detect loci persistently implicated in beak shape evolution across lineages by integrating morphological data into substitution rate models in a phylogenetic framework. We analysed protein coding genes as well as noncoding conserved regions from 72 bird species and combined them with morphological information from all major avian orders and families spanning >97% of avian genera (Cooney et al. 2017). Using this approach, we were able to link genetic and morphological diversification on a macroevolutionary scale.

Results

Previous work has identified several genes and genomic regions that are under selection as likely species-specific drivers of bird beak shape evolution (Table S1). In order to identify genes that play a role in beak shape evolution beyond a lineage or species specific scale, we performed sequence divergence analyses on protein coding genes and avian-specific highly conserved elements, possibly regulatory, regions.

Detecting protein coding genes repeatedly implicated in beak shape evolution

To test whether protein coding changes of the same protein are repeatedly implicated with beak shape morphological change across taxa, we designed an approach that incorporates estimates of morphological trait evolution into a branch model of sequence diversification. Specifically, we estimated sequence divergence using the ratio of non-synonymous substitutions to synonymous substitutions ($d_{\mathrm{N}}/d_{\mathrm{S}}$), which provides an indication of selection acting at the protein level. Our model assumes that the rate of molecular evolution ($d_{\mathrm{N}}/d_{\mathrm{S}}$) varies between predetermined types of branches, but not between sites in a protein, which is a reasonable restriction for computational reasons (Yang 1998; Yang and Nielsen 1998). We obtained estimates of rates of beak shape evolution based on geometric-morphometric data for all branches and grouped them into ranked bins according to their respective rates of beak shape evolution (Figure 1). If protein coding genes drive morphological change we hypothesised a positive correlation

between ranked bins – where bins increased in rates of estimated phenotypic evolution incrementally – and estimates of d_N/d_S. For the 10,238 genes included in our analysis, we set up a branch model assuming different d_N/d_S for each bin. Accompanying this, for each binned model, we estimated d_N/d_S in a null model assuming no difference in d_N/d_S between bins. A comparison between the binned model and the null model using a likelihood ratio test will reveal whether there is significant variation in the rate of protein change across our grouped branches.

We found that 1,434 ($\approx$ 14%) genes had significant variation in their d_N/d_S values across the grouped branches after correcting for multiple testing (e.g. significantly different likelihoods between the two models, FDR < 0.05). To determine putative functions of these genes, we performed phenotype ontology and pathway enrichment analyses using WebGestalt (Wang et al. 2017). Among the most enriched pathways are *Wnt Signalling pathway* and *ESC pluripotency pathways* (Figure 2A), both of which have been implicated in beak morphological development (Wu et al. 2004; Abzhanov et al. 2004; Merrill et al. 2008; Brugmann et al. 2010). Among the top phenotypic ontologies we find several ontology descriptions associated with skin as well as ectopic calcification and hydrocephalus (Table 1). We also used STRING (Szklarczyk et al. 2015), a comprehensive database combining different evidence channels for protein-protein interaction networks and functional enrichment analysis, to identify protein interaction partners of three proteins that have been previously identified as being associated with bird beak shape morphology independent of size effects (ALX1, BMP4 and CALM1, Table S1). ALX1, in contrast to BMP4 and CALM1, shows only two predicted interaction partners while the other two proteins are part of huge interaction networks (Figure S1). Altogether we identified 467 protein interaction partners across the three proteins and tested whether there is an enrichment of these in our dataset of 1,434 genes, which is indeed the case (Table 2, χ^2 test, df=1, P=0.002).

We hypothesized a positive correlation between rates of molecular change and beak shape change, however after correcting for multiple testing no significant correlations were observed. This might be caused by limited power, e.g. due to short gene length or branch length, but generally suggests limited evidence for a simple relationship between the rate of molecular change in protein coding genes and morphological change.

Detecting conserved noncoding regions implicated in beak shape evolution

To identify noncoding, possibly regulatory, regions that may be associated with beak shape morphological change over macroevolutionary time we analysed genomic regions based on avian conserved elements obtained from the chicken genome (Seki et al. 2017). Specifically, we obtained multiple sequence alignments of conserved regions from whole genome alignments comprising 72 bird genomes (Table S2) and grouped branches in up to 16 different categories using a *k*-means binning approach on branch specific morphological beak shape rate change (Cooney et al. 2017), a similar binning approach as for protein coding genes. Simulations show that 16 bins capture rate heterogeneity among branches very well at computationally feasible costs (Figure S2).

We successfully processed and analysed 229,001 conserved elements, of which 39,806 ($\approx$ 17.4%) showed significant variation in their substitution rates after correcting for multiple testing (χ^2-test, FDR<0.05). As we were interested to link potentially cis-regulatory elements to their target genes we restricted our analysis to conserved elements within or in close proximity to genes. Although the location of cis-regulatory elements is not fixed, they frequently occur in introns (Wittkopp and Kalay 2012) or close to the transcription start site, such as promoters and promoter-proximal elements (Butler and Kadonaga 2002; Andersson and Sandelin 2020). We extracted 884 genes that were overlapping or within 200bp distance (Piechota et al. 2010) of the identified regions in the chicken genome. To determine putative functions of these genes, we performed phenotype ontology and pathway enrichment analyses using WebGestalt (Wang et al. 2017). Among the most enriched pathways are *Ectoderm Differentiation*, *Mesodermal Commitment Pathway*, *Focal adhesion* and the *ESC Pluripotency pathways* (Figure 2B). The latter pathway set was also identified for the protein coding genes and represents an ensemble of pathways, including BMP and Wnt signalling, necessary for regulating pluripotency of embryonic stem cells (Okita and Yamanaka 2006). Phenotypic associations included “Abnormality of mouth shape and nasal bridge”, “cleft upper lip” and “nyctalopia” (Table 1).

We find that the 884 protein coding genes in cis to the identified genomic regions are overrepresented in a set of 511 genes involved in early craniofacial development in mice (Brunskill et al. 2014) (P=0.012, χ^2-test, df=1, Table 3). To investigate whether there is any indicator for a biological meaningful relationship of the rate of molecular change and the rate of morphological change we focused on 2,644

out of 39,806 genomic regions ($\approx$ 1.2% of all genomic regions) that individually showed a significant correlation (Kendall τ, P<0.05) between beak shape rates and substitution rate. We find that the over-representation for mice craniofacial genes is driven by a subset of 163 genes nearby the 2,644 regions (P=2.5$\times 10^{-5}$, χ^2-test), but not the 721 remaining genes (P=0.58, χ^2-test, df=1). This suggests that the rate of molecular change in noncoding regions may be correlated to the rate of beak shape change (Table 3).

These previous analyses are most likely to identify the role of cis-regulatory elements because they focus on genes nearby to noncoding regions. Hence, we conducted a second strategy to gain further insights into the role of the identified noncoding regions as possible trans-acting elements. For this, we searched for short enriched motifs in the set of 39,806 genomic regions using DREME (Bailey 2011), and focused on the top 20 enriched motifs (Table S3). These motifs are potentially part of genomic regions that are targets of transcription factors.

To identify potential proteins binding to these motifs we used TOMTOM (Gupta et al. 2007) and obtained 145 potential annotated binding proteins, including GSC and SMAD proteins, both previously identified to be associated with beak shape morphological evolution (Parsons and Albertson 2009; Lamichhaney et al. 2015). To discern potential functions related to craniofacial features we conducted a phenotype enrichment analysis and identified “Abnormal lip morphology” as significant phenotype association and “lip and craniofacial abnormalities” as disease associated ontologies using a disease annotation database (Table 1).

Genetic differentiation of the identified noncoding loci in Darwin’s finches

To test whether the identified noncoding loci may play a role in shaping beak morphology in a recent diversification we obtained polymorphism data from Darwin’s finch populations that either show a pointy or blunt beak phenotype (Lamichhaney et al. 2015). Using this dataset we find that our identified regions are characterised by patterns of linked selection that differ to a genomic control. Relative to genomic control regions, we find a stronger genetic differentiation between blunt and pointy phenotype populations (Figure 3A), as well as a higher overall genetic diversity at our identified loci (Figure 3B).

Genes underlying evolutionary hotspots of beak shape divergence

Major evolutionary changes in beak shape may be concentrated within specific time periods and/or lineages (Cooney et al. 2017), and it is plausible that genes underlying these changes will show corresponding signatures of rapid evolution associated with such instances of 'quantum evolution' (Simpson 1944). We tested this prediction by identifying branches with the fastest-evolving rates of beak shape evolution according to trait evolution estimates derived from our morphological data. We selected three branches in our phylogeny with the most divergent beak shape evolution and refer to these branches as 'hotspots' (Figure S3). We conducted branch model tests (Yang et al. 1998; Yang 1998) for each of the three rapidly-evolving branches.

After accounting for multiple testing, we detected 36 genes with a signature of rapid evolution (d_N/d_S > 1, Figure 4). Although d_N/d_S>1 is indicative of rapid evolution, a formal significance test (versus a model with a fixed d_N/d_S=1 for the tested branch) suggests only for nine of our 36 identified genes a significant elevation of d_N/d_S above one, indicative of positive selection (Figure 4). We identified BGLAP, a gene encoding osteocalcin, a highly-abundant, non-collagenous protein found in embryonic bone and involved in bone formation (Ducy et al. 1996; Raymond MH, Schutte BC, Torner JC, Burns TL 1999). Furthermore, we identified SOX5, a gene reported to have an assistive role in regulating embryonic cartilage formation (Lefebvre et al. 1998). In chickens, the expression of SOX5 and a duplication in the first intronic region of the gene is associated with the Pea-comb phenotype (Wright et al. 2009).

Discussion

We developed a phylogenetic approach to identify genomic loci underlying the evolution of beak shape across macroevolutionary time and investigated genetic changes at coding and noncoding DNA across 72 bird species. Specifically, we asked whether loci that are repeatedly implicated in beak shape evolution across the bird phylogeny can be detected. By binning branches according to estimated rates of beak shape evolution, on the basis that phenotypic evolution is informative of genetic changes, we estimated rates of protein evolution across more than 10,000 genes, as well as rates of DNA substitutions for more than 200,000 avian-specific conserved regions, in a phylogenetic context.

Protein coding genes associated with beak shape evolution across birds

For protein coding genes, we found significant variation in d_N/d_S between binned branches in $\approx$ 14% of the genes tested, but we did not find a significant correlation between rates of phenotypic evolution and protein evolution for any gene. The binned model for coding DNA described in this study is not a formal test for positive selection, however a positive correlation between evolutionary rates and morphological genes could be indicative of repeated adaptive evolution of the same gene. Although we do not find evidence for this, some loci may have experienced shifts in d_N/d_S ratios repeatedly across distantly-related branches in association with beak shape morphological change. This relation may be explained by a number of different evolutionary forces, potentially acting independently or in tandem.

An association between d_N/d_S and morphological changes may not be associated with adaptive events, but could also be explained by varying levels of genetic drift or purifying selection. For instance, relaxed purifying selection often occurs in response to environmental changes that weaken the effect of selection previously required to maintain a trait (Lahti et al. 2009). Furthermore, environments and therefore selective pressures are unlikely to remain stable over long evolutionary times. So far, only a few analyses have found experimental evidence of fluctuating selection acting on polymorphisms (Lynch 1987; O'Hara 2005). However, at a broader scale, models estimating the effects of fluctuating selection suggest a contribution to divergence similar to signatures of adaptive evolution (Huerta-Sanchez et al. 2008; Gossmann et al. 2014). Depending on the strength of fluctuating selection, or other types of varying selection intensities, it may account for the lack of strong, positive correlation coefficients reported in this study.

Although we might generally expect that morphological change in beak shape is positively correlated with d_N/d_S, an alternative scenario can explain a negative correlation. Adaptive mutations, because of their functional importance, are expected to experience strong purifying selection after their fixation (Kimura 1983). Functionally-important genes typically show signals of strong purifying selection ($d_N/d_S << 1$) and this is not conducive to a pattern of repeated increase in d_N/d_S over distantly-related branches. Instead, a selective sweep would be followed by sustained reduction in d_N/d_S through a prolonged period of intense purifying selection. We also did not identify genes with a significant negative correlations. We want to stress that further exploration of how adaptation occurs over macroevolutionary time, and the

signals of selection left by ancient adaptive events is necessary to be able to fully elucidate our results. It may well be that our assumption of a positive correlation with beak shape rate does not hold because the role of convergent evolution is less pervasive, or that a rate analysis at coding sites does not have enough power as a measure of repeated directional positive selection.

The effect of varying effective population size and life-history traits

Following the K-Pg extinction, modern birds experienced drastic reductions in body size, and with it, an increase in shorter generation time – this phenomenon is termed the Lilliput effect (Berv and Field 2018). Critically, reductions in body size and generation time have likely resulted in an increased N_e, and alongside it, an increase in the efficacy of selection (Kimura 1983; Gossmann et al. 2010; Lanfear et al. 2014). This gradual decrease in body size and generation time, and with it, an increase in the neutral substitution rate, could account for an incremental decrease in $d_{\mathrm{N}}/d_{\mathrm{S}}$ over time. So far, a number of studies have reported that a relationship exists between body mass and rates of molecular evolution in birds, with varying results (Weber et al. 2014; Nabholz et al. 2016; Botero-Castro et al. 2017; Figuet et al. 2017). In apparent contradiction with expectations of the neutral theory, several studies found that a decrease in body mass in birds did not result in decreased $d_{\mathrm{N}}/d_{\mathrm{S}}$ estimates (Lanfear et al. 2010; Nabholz et al. 2013; Weber et al. 2014; Bolívar et al. 2019). In fact, they found a weakly negative relationship between body mass and $d_{\mathrm{N}}/d_{\mathrm{S}}$, although similar studies report the opposite trend: $d_{\mathrm{N}}/d_{\mathrm{S}}$ in birds is positively correlated with body mass (Botero-Castro et al. 2017; Figuet et al. 2017). Indeed, mean and median correlation coefficient of $d_{\mathrm{N}}/d_{\mathrm{S}}$ with beak shape rate change is 0.047 and 0.048, respectively (significantly different from zero, P<<0.05, one sample *t*-test, n=1,434), for the 1,434 genes with significant heterogeneity in $d_{\mathrm{N}}/d_{\mathrm{S}}$, possibly suggesting a co-variation of beak shape change with other traits, such as body size.

Fluctuations in effective population size (N_e), which are not taken into consideration by models of protein evolution, may affect interpretations of $d_{\mathrm{N}}/d_{\mathrm{S}}$. For example, fluctuations in N_e may cause the fixation of neutral or slightly-deleterious mutations – in this case, this would mean the interpretation that $d_{\mathrm{N}}/d_{\mathrm{S}}$ > 1 is indicative of positive or diversifying selection may be erroneous. Strong shifts in $d_{\mathrm{N}}/d_{\mathrm{S}}$ may be driven by sudden changes in population size or genuine positive selection, and might obscure or oppose incremental increases in $d_{\mathrm{N}}/d_{\mathrm{S}}$ across bins (Bielawski et al. 2016; Jones et al. 2016). In our

model, however, the effects of population size changes are partially negated by co-estimating parameters across branches. Unless specifically accounted for, substitution rate models do not consider the effect of non-equilibria processes that could affect d_N/d_S estimates (Matsumoto et al. 2015). For example, GC-biased gene conversion - described as the preferential conversion of 'A' or 'T' alleles to 'G' or 'C' during recombination induced repair – has been shown to significantly affect estimates of substitution rates, in particular at synonymous sites in birds (Galtier et al. 2009; Weber et al. 2014; Bolívar et al. 2016; Botero-Castro et al. 2017; Corcoran et al. 2017; Bolívar et al. 2019). However, while differences in the extent of GC biased gene conversion across genes are known, much less is known about its variation over time and incorporating such biases into large scale phylogenetic frameworks is far from trivial (Gossmann et al. 2018).

Noncoding regions associated with beak shape morphology evolution across birds

Branch specific substitution rates of more than 39,000 avian-specific conserved regions are significantly associated with beak shape rates. We find more than 850 genes that are nearby these regions, possibly cis-regulatory factors, that show significant enrichment for craniofacial phenotypes in humans and mice. Unlike for protein coding regions we were unable to correct our substitution rate estimates for the effect of varying mutation rates (e.g. there is no counterpart for d_S as for coding regions). Due to special features of the avian karyotype, such as a stable recombinational and mutational landscape, it seems unlikely that variation in mutation rate can contribute to the patterns observed here. However, while inter-chromosomal re-arrangements are rare in birds, intra-chromosomal changes are more common and could lead to sudden changes in local mutation rates (Gossmann et al. 2018). Additionally, we restricted our analysis to noncoding regions that are specific to birds, or highly divergent relative to vertebrates (Seki et al. 2017). Whether anciently conserved elements, such as vertebrate specific regulatory regions (Lowe et al. 2015), may play a role in avian beak shape remains an open question. Equally, as the noncoding regions were identified based on the chicken genome, we lack those conserved regions that are absent from the chicken genome but present in other parts of the phylogeny.

More than 2,000 of the identified regions showed a significant correlation with binned rates of beak shape change and genes nearby these regions significantly overlap with genes involved in craniofacical development in mice (Table 3). The association of sequence divergence and trait divergence, along with

a strong phenotypic enrichment, might suggest that the accumulation of neutral mutations at noncoding sites may play a pronounced role in bird beak diversification. This is because in our applied model we cannot distinguish between the action of selection and the accumulation of drift through fixations of new mutations (e.g. background variation in mutation rate). Hence, disentangling differences in the evolutionary pressures these regions experienced remains a major future challenge.

Some of the noncoding conserved genomic regions we identified may not be in physical proximity to a gene, e.g. many enhancers can be megabases away from the gene they regulate. Potentially, this could result from missing annotation for the *Gallus gallus* genome, or the fact that the genomic regions are trans-acting factors. Identifying the mechanisms underlying trans-acting factors is however very difficult to approach *in-vitro* as well as *in-silico*, and our approach to detect the role of trans-acting factors over macroevolutionary time is novel. We opted for an *in-silico* approach through motif enrichment and harvested vertebrate DNA binding protein databases to identify DNA binding proteins involved in beak diversification that go beyond a cis-acting role. We identified 145 possible DNA binding proteins using WebGestalt, including known transcription factors shown to be involved in beak development, that might be associated with beak shape diversification.

Although there is some overlap between the identified protein coding gene set and the noncoding gene set (Figure 5A), this is substantially less than expected by chance (P<0.005, χ^2-test, df=1, protein coding genes versus genes near noncoding regions, Figure 5B). Indeed, based on the pathway and phenotype associations we note that the identified ontologies are different between the two datasets (Table 1). Although genes nearby noncoding regions are associated with facial and anatomical features, such as mouth shape, cleft and nasal abnormalities, the protein-coding phenotypes are mainly associated with dermal features. This suggests that the underlying evolutionary mechanisms of protein coding genes and noncoding, potentially regulatory, regions may be rather distinct in beak morphology evolution. However, as a common pattern, we identified that the ESC pathways are enriched in the coding and noncoding gene sets (Figure 5C). This further supports the notion that fundamental cellular pathways, such as BMP and Wnt signalling pathways, play a crucial role in the development of bird beaks and that this signal is detectable at a macroevolutionary scale.

A pressing question remains as to whether these long-term associations are also reflected in selection at the micro-evolutionary level (Shultz and Sackton 2019). To test this we obtained data from Darwin's

finch populations that differ in their beak shape morphology (Lamichhaney et al. 2015). Our identified regions are characterised by pattern of linked selection that differ from genomic control regions with stronger genetic differentiation between blunt and pointy phenotype populations (Figure 3A), as well as a higher overall genetic diversity at our identified loci, suggestive of diversifying or partially relaxed purifying selection (Figure 3B). The signatures of selection are embedded in a genetic environment that shows local reduction of diversity due to strong purifying selection at these regions, typical of highly conserved regions. Sophisticated analyses of pinpointed genomic loci will be pivotal for future studies to disentangle the selective forces at these sites.

Rapid genetic evolution in hotspots of beak shape evolution

In a second approach we focused on the findings of previous studies: beak shape changes are driven by different genes in specific branches. Applying this rationale, we identified rapidly-evolving lineages from comprehensive trait evolution analyses specifically focused on beak shape evolution (Cooney et al. 2017), and tested genes at these branches for accelerated rates of corresponding protein evolution. We identified 36 protein coding genes with branch specific signals of rapid evolution, with nine of them showing evidence for positive selection. These genes are putatively linked to branch and lineage-specific changes in beak morphology.

The most plausible candidates were detected in an internal branch leading to the evolution of the Strisores, a clade estimated to have diverged over 60 MYA, comprised of swifts, hummingbirds, nightjars and their allies (Hackett et al. 2008; Prum et al. 2015; Cooney et al. 2017). As well as distinctively short beaks evolving in swifts and nightjars, the divergence of hummingbirds is characterized by significant changes beak shape, body size and metabolism. This is supported by reported accelerated rates of evolutionary change in multiple cranial modules in Strisores (Felice and Goswami 2017). Together, these changes encapsulate adaptive shifts that have occurred in the Strisores clade.

An important candidate that may explain some of these changes is *BGLAP*, a gene encoding for osteocalcin, a ubiquitous protein found in bones and whose presence is critical for normal bone development (Ducy et al. 1996). Instead of direct involvement in bone production, osteocalcin regulates insulin expression and excretion, thereby regulating energy expenditure in muscle tissue, development of bone

tissue and insulin sensitivity (Lee et al. 2007; Karsenty and Ferron 2012; Mera et al. 2016). Equally, as with *COL4A5*, a type IV collagen protein encoding gene, and *ALX1*, implicated in craniofacial development in Darwin's finches, *BGLAP* may alternatively play a role in beak shape evolution (Lamichhaney et al. 2015; Bosse et al. 2017b).

Similarly, we identified *SOX5*, a gene previously associated with the evolution of craniofacial phenotypes in chickens, to be under putative positive selection in Strisores (Wright et al. 2009). Specifically, pea-comb development is associated with ectopic expression of *SOX5* caused by copy-number variation at the first intron of *SOX5* (Wright et al. 2009). This is independently corroborated by strong expression patterns of *SOX5* in the brain tissue – a possible proxy for craniofacial tissue, which is not included in expression profiles – of chickens (Merkin et al. 2012). Beyond the pea-comb phenotype, SOX5 is an essential transcription factor that acts to regulate chondrogenesis by enhancing a type-2 collage protein (COL2A1) and promotes the differentiation of chondrocytes. Critically, the expression pattern of *COL2A1* in the pre-nasal cartilage, an important morphological module of beaks and their shape(s), explains beak shape differences between medium and large ground finches during the 27th embryonic stage of development (Mallarino et al. 2011). Therefore, we suspect that *SOX5* may be important in explaining beak shape changes in swifts, hummingbirds and nightjars.

Beak shape as a proxy for trait diversification

A key principle of adaptive radiation theory is that diversification of species is associated with ecological and morphological diversity (Schluter 2000). In birds, the evolution of morphological changes tends to coincide with speciation events, with some discontinuities, particularly early on in avian evolution (Foote 1997; Ricklefs 2004; Hughes et al. 2013; Mcentee et al. 2018). Here, we focus particularly on beak shape evolution because of its putative importance as a key ecomorphological trait and its link to speciation, demonstrated by long term trends and direct ecological evidence in Darwin's finches (Cooney et al. 2017; Ricklefs 2004; Mcentee et al. 2018; Lamichhaney et al. 2018; Han et al. 2017; Grant and Grant 2009; Podos 2001; Huber and Podos 2006). However, evidently, many of the genes detected in this study are not associated with beak shape according to their putative functions. There are two explanations for this: First, some of the identified genes are pleiotropic in character and second, their functions are associated with traits that co-vary with beak shape evolution. We suspect that, alongside

strong candidates for beak shape, we have detected genes implicated in a range of adaptive changes that have allowed species to diversify into different ecological niches. Here, estimates of beak shape evolution taken from Cooney et al. (2017) may have acted to identify branches with the fastest rate of phenotypic evolution rather than beak shape evolution specifically. This may be of particular relevance for the identification of genomic loci underlying beak shape diversification hotspots.

In summary, we were able to identify genomic loci associated with beak shape morphological evolution over macroevolutionary time by combining morphometric analyses with genomic data. For both, coding and noncoding regions, less than 20% of the tested loci show significant variation in their molecular rates, and most of the tested loci in this study are genetically very conserved on a macroevolutionary scale and hence cannot provide a genetic explanation for the observed phenotypic variation in beak shape across species. We show that homologs of identified protein coding genes as well as genes in close proximity to identified noncoding regions, are involved in craniofacial embryo development in mammals and pinpoint two associated pathways, BMP and Wnt signalling, illustrating that changes in coding as well as noncoding DNA facilitate phenotypic evolution of avian beak shape. The identified coding and noncoding loci are highly distinct, with significantly reduced overlap between them and fundamentally different phenotype associations. At present, the selective forces that contribute to patterns of genetic and morphological diversification remain difficult to pinpoint. However, as genomic and morphological data continue to accumulate, our framework offers a potentially powerful approach to further disentangling the interplay of selection and drift responsible for driving the diversification of complex phenotypic traits at macroevolutionary scales.

Methods

Multiple sequence alignments for protein coding genes

We used genomes of 57 bird species with high quality annotations from NCBI RefSeq (O'Leary et al. 2016) (Table S2). First, 12,013 orthologous protein coding genes were retrieved using RefSeq and HGNC gene identifiers, alongside reciprocal BLAST approaches based on three focal species, chicken, great tit and zebra finch - three of the best annotated high quality bird genomes available to date (Li et al. 2003; Östlund et al. 2009; Afanasyeva et al. 2018). We then performed a first set of alignment runs

using PRANK (Löytynoja and Goldman 2008). To ensure the quality of these sequence alignments, we applied a customised pipeline including multiple alignment steps and quality filters. Details are described in the Supplemental Methods.

Avian specific highly conserved regions (ASHCE) alignments derived from multispecies whole genome alignments

To estimate substitution rates for noncoding conserved elements across the bird phylogeny, we obtained whole genome information from NCBI for 72 bird species including the 57 bird species using in the coding DNA analysis. To generate a multispecies whole genome alignment we aligned the 72 avian reference genomes (as of 15/2/2017) against version 3 (galGal3) of the chicken (*G. gallus*) genome (version: galGal3 available from: ftp://ftp.ensembl.org/pub/release-54/fasta/gallus_gallus/dna/) using the MULTIZ package (Blanchette et al. 2004). Alignments were performed per chromosome following a pipeline published earlier (Corcoran et al. 2017). A list of query species, genome versions used and download locations can be found in Table S2. We used avian-specific highly conserved elements (ASHCE) from Seki et al. (2017). They used whole-genome alignments for 48 avian and 9 non-avian vertebrate species spanning reptile, mammal, amphibian and fish to obtain 265,984 ASHCEs. We were able to prepare 229,001 (86% of the total number of ASHCE) high-quality alignments as input for the analysis with baseml. For this target ASHCE regions were intersected with the whole genome alignments using BEDTools (v2.27.0) and FASTA files were created using customised scripts. Spurious and poorly aligned sequences were automatically removed using trimAl v1.4 (Capella-Gutierrez et al. 2009).

Rates of morphological beak shape evolution

Information on beak shape evolution was extracted from a recent study (Cooney et al. 2017) that quantified patterns of beak shape evolution across 2,028 species (>97% extant avian genera) covering the entire breadth of the avian clade. Briefly, this study used geometric morphometric data based on 3-D scans of museum specimens and multivariate rate heterogeneous models of trait evolution (Venditti et al. 2011) to estimate rates of beak shape evolution for all major branches in the avian phylogeny.

Based on this information, we hypothesised that branches found to have experienced rapid beak shape

evolution should also experience faster evolutionary change at the protein or genomic level. To test this, we split our evolutionary analyses into two, discrete approaches. First, for the detection of genes and genomic regions that have recurring effects on beak shape variation across multiple branches, we devised a binned approach. Second, for the detection of genes undergoing positive selection at branches that show rapid morphological change, we designed a hotspot approach.

Binned branch approach for the detection of large-effect genes and regulatory regions

To detect genes that may be undergoing repeated periods of rapid, possibly adaptive, evolution across multiple lineages, we grouped branches in each alignment phylogeny according to their rates of morphological evolution using *k*-means binning (Lloyd 1982). Here, we opted for up to eight (coding) and 16 (ASCHE) bins, respectively, to enable robust statistical analysis but still reasonable computational time for the substitution rate analysis. To phylogenetically link the genetic data to the morphological data we relied on the Hackett et al. backbone (Hackett et al. 2008), hence we did not account for phylogenetic heterogeneity among genes and possible gene-tree species tree discordance. Branches were grouped incrementally based on rates of trait evolution using a *k*-means binning approach, with the first bin representing branches with the slowest rates of morphological evolution, and the last bin representing branches with the fastest rates of morphological evolution (Figure 1). We assumed that genes involved in beak shape evolution would experience evolutionary rate change at the protein level ($d_{\mathrm{N}}/d_{\mathrm{S}}$) proportional to their respective rate of morphological evolution. Theoretically, we hypothesize that genes important in beak shape evolution across many branches would show a strong positive correlation.

In our analysis, we tested this using a branch model which assumes different substitution rates ($d_{\mathrm{N}}/d_{\mathrm{S}}$) across different, pre-defined, branches in a phylogeny. Critically, the branch model may be useful in the detection of adaptive evolution occurring on particular branches (Yang et al. 1998; Yang 1998). Furthermore, we selected the branch model due to computational efficiency; the branch-site model and free-ratio model was deemed computationally intractable for a phylogeny of up to 57 species. Branches in each alignment's phylogeny were marked according to their respective bins (typically ranging from 1 to 8). Labelling bins as distinct types of branches allowed for the estimation of up to eight different $d_{\mathrm{N}}/d_{\mathrm{S}}$ values per gene. Conjointly, for each binned model, an alternative null model assuming no difference in $d_{\mathrm{N}}/d_{\mathrm{S}}$ between branches was run (one-ratio model). The difference between models was compared us-

ing a likelihood-ratio test (LRT) by comparing twice the log-likelihood difference between the two models which is assumed to be χ^2 distributed, with the relevant degrees of freedom (Yang 2007).

To estimate rate hetereogeneity among branches in noncoding regions, we used a model where we assumed equal rates among branches (e.g. a global clock, clock=1) and compared it to a model where we assumed different rates for the binned branches (clock=2), assessing significant differences between the models using a likelihood ratio test. For the simulations (Figure S2) we randomly chose a 222bp long genomic region with 67 species. We run a free branch model (clock=0) and used the obtained parameters as input for INDELible (Fletcher and Yang 2009). We simulated 100 sets of sequences and applied two types of binning: (1) A binning that grouped similar branch lengths and (2) an arbitrary binning. We considered 5 different numbers of bins (with 2,4,8,16 and unrestricted number of bins). We then conducted rate estimation on each of the binning approaches and calculated how well these estimates correlated (Kendall's τ correlation coefficient) with the input parameters for INDELible (e.g. the simulation input) as well as the estimated values from the free branch model.

Hotspot approach for the detection of genes under positive selection

To formally test for rapid and potentially positive selection on branches with increased rates of morphological evolution, we used a 'hotspot' approach. As opposed to focusing on large-effect genes important across distantly-related avian taxa, we identified and marked specific, individual branches undergoing the fastest rates of morphological evolution, according to rate estimates from Cooney et al. (2017). At these branches, we hypothesize to detect higher $d_{\mathrm{N}}/d_{\mathrm{S}}$ estimates relative to background branches.

Phenotype and pathway ontologies, protein databases and statistical analyses

To determine the putative function of genes detected and enriched according to pathway and phenotype enrichment, we used WebGestalt (Wang et al. 2017) based on the human annotation. Specifically, we used the latest release of WebGestalt (last accessed 11.3.2019), and ran an Overrepresentation Enrichment Analysis (ORA) for phenotypes (Human Phenotype Ontology), pathways (Wikipathways) and diseases (Glad4U). We set the minimum number of genes for a category to 40 and reported top statistical significant results as weighted cover set (as implemented in WebGestalt). We also obtained a set of

511 genes known from mouse knock-out phenotypes to result in abnormal craniofacial morphology or development (Brunskill et al. 2014). To account for multiple testing in our binned and hotspot models, χ^2-squared P-values were corrected using the Benjamini-Hochberg procedure (Benjamini and Hochberg 1995). We used Kendall's τ correlation coefficient to compare the association between increasing bin number and corresponding $d_{\mathrm{N}}/d_{\mathrm{S}}$ (coding) and substitution rates (noncoding) for each gene. Statistical analysis was conducted using the SciPy library in Python, and graphs were produced using the 'tidyverse' package in R (Wilkinson 2011; R Core Team 2018) and the 'matplotlib' package in Python. Phylogenies were produced using the 'phytools' package in R (Revell 2012). Protein interaction partners for ALX1, BMP1 and CALM1 were retrieved from the STRING database (Szklarczyk et al. 2015) based on the human annotation requiring a minimum confidence score of 0.6 for all interaction partners. Motif detection was conducted using DREME (Bailey 2011) along with the identification of potential binding proteins using TOMTOM (Gupta et al. 2007). Specifically, we focused on vertebrate binding proteins using a common set of three available databases (JASPAR2018_CORE_vertebrates_non-redundant, jolma2013, uniprobe_mouse) that together contained 649 annotated motif binding proteins.

Population genetic analysis in Darwin's finches population with diverse beak morphology

We obtained per site measurements of population differentiation (fixation index F_{ST} and nucleotide diversity θ (Watterson 1975; Weir and Cockerham 1984) by calculating and contrasting genetic diversity of Darwin finch populations (Lamichhaney et al. 2015) with blunt (5 and 10 individuals from *Geospiza magnirostris* and *G. conirostris* populations, respectively) and pointed beaks (10 and 8 individuals from *G. conirostris* and *G. difficilis* populations, respectively).

Software availability

Scripts concerning the analysis of protein coding regions and noncoding regions are available at GitHub (https://github.com/LeebanY/avian-comparative-genomics; https://githubcom/mattheatley/bird_project) and as Supplemental Code.

Acknowledgements

We thank Sangeet Lamichhaney for providing F_{ST} data on the Darwin finch populations and Victor Soria-Carrasco, Gavin Thomas and Jon Slate for constructive comments at earlier stages of this work. We also want to thank Ahmet Denli and three anonymous reviewers for their comments that helped to improve the quality of this work.

Funding information: TIG is supported by a Leverhulme Early Career Fellowship (Grant ECF-2015-453) and a NERC grant (NE/N013832/1), CRC is supported by a Leverhulme Early Career Fellowship (ECF-2018-101) and MH is supported by an BBSRC summer project placement funding.

Author Contributions: LY drafted the manuscript; TIG and CRC designed and supervised the study; TIG, LY, MH and JP conducted research; HJB contributed to research; TIG finalized the manuscript with written input from all authors

Competing interests: The authors declare that they have no competing interests.

References

Abzhanov A, Kuo WP, Hartmann C, Grant BR, Grant PR, Tabin CJ. 2006. The calmodulin pathway and evolution of elongated beak morphology in Darwin's finches. *Nature* **442**: 563–567.

Abzhanov A, Protas M, Grant BR, Grant PR, Tabin CJ. 2004. Bmp4 and morphological variation of beaks in Darwin's finches. *Science* **305**: 1462–1465. http://www.ncbi.nlm.nih.gov/pubmed/15353802.

Afanasyeva A, Bockwoldt M, Cooney CR, Heiland I, Gossmann TI. 2018. Human long intrinsically disordered protein regions are frequent targets of positive selection. *Genome research* **28**: 975–982. http://www.ncbi.nlm.nih.gov/pubmed/29858274
http://www.pubmedcentral.nih.gov/articlerender.fcgi?artid=PMC6028134.

Andersson R, Sandelin A. 2020. Determinants of enhancer and promoter activities of regulatory elements. **21**: 71–87.

Bailey TL. 2011. DREME: motif discovery in transcription factor ChIP-seq data. *Bioinformatics* **27**: 1653–1659. https://academic.oup.com/bioinformatics/article-lookup/doi/10.1093/bioinformatics/btr261.

Balanoff AM, Bever GS, Rowe TB, Norell MA. 2013. Evolutionary origins of the avian brain. *Nature* **501**: 93–96. http://dx.doi.org/10.1038/nature12424.

Benjamini Y, Hochberg Y. 1995. Controlling the false discovery rate: a practical and powerful approach to multiple testing. *Journal of the Royal Statistical Society Series B (Methodological)*.

Berv JS, Field DJ. 2018. Genomic Signature of an Avian Lilliput Effect across the K-Pg Extinction. *Systematic Biology* **67**: 1–13.

Bhullar AB-aS, Morris ZS, Sefton EM, Bhullar B-aS, Morris ZS, Sefton EM, Tok A, Tokita M, Namkoong

B, Camacho J, et al. 2015. A molecular mechanism for the origin of a key evolutionary innovation , the bird beak and palate , revealed by an integrative approach to major transitions in vertebrate history. 1665–1677.

Bhullar B-AS, Hanson M, Fabbri M, Pritchard A, Bever GS, Hoffman E. 2016. How to Make a Bird Skull: Major Transitions in the Evolution of the Avian Cranium, Paedomorphosis, and the Beak as a Surrogate Hand. *Integrative and Comparative Biology* **56**: 389–403. https://academic.oup.com/icb/article-lookup/doi/10.1093/icb/icw069.

Bhullar B-AS, Marugán-Lobón J, Racimo F, Bever GS, Rowe TB, Norell MA, Abzhanov A. 2012. Birds have paedomorphic dinosaur skulls. *Nature* **487**: 223–226. http://www.nature.com/articles/nature11146.

Bielawski JP, Baker JL, Mingrone J. 2016. Inference of Episodic Changes in Natural Selection Acting on Protein Coding Sequences via CODEML. In *Current protocols in bioinformatics*, Vol. 54 of, pp. 6.15.1–6.15.32, John Wiley & Sons, Inc., Hoboken, NJ, USA http://doi.wiley.com/10.1002/cpbi.2.

Blanchette M, Kent WJ, Riemer C, Elnitski L, Smit AFA, Roskin KM, Baertsch R, Rosenbloom K, Clawson H, Green ED, et al. 2004. Aligning multiple genomic sequences with the threaded blockset aligner. *Genome research* **14**: 708–15. http://www.ncbi.nlm.nih.gov/pubmed/15060014 http://www.pubmedcentral.nih.gov/articlerender.fcgi?artid=PMC383317.

Bolívar P, Guéguen L, Duret L, Ellegren H, Mugal CF. 2019. GC-biased gene conversion conceals the prediction of the nearly neutral theory in avian genomes. *Genome Biology* **20**: 5. https://genomebiology.biomedcentral.com/articles/10.1186/s13059-018-1613-z.

Boĺivar P, Mugal CF, Nater A, Ellegren H. 2016. Recombination rate variation modulates gene sequence evolution mainly via GC-Biased gene conversion, not Hill-Robertson interference, in an avian system. *Molecular Biology and Evolution* **33**: 216–227.

Bosse M, Spurgin LG, Laine VN, Cole EF, Firth JA, Gienapp P, Gosler AG, McMahon K, Poissant J, Verhagen I, et al. 2017a. Recent natural selection causes adaptive evolution of an avian polygenic trait. *Science* **358**: 365–368.

Bosse M, Spurgin LG, Laine VN, Cole EF, Firth JA, Gienapp P, Gosler AG, McMahon K, Poissant J, Verhagen I, et al. 2017b. Recent natural selection causes adaptive evolution of an avian polygenic trait. *Science*.

Botero-Castro F, Figuet E, Tilak M-k, Nabholz B, Galtier N. 2017. Avian genomes revisited: hidden genes uncovered and the rates vs. traits paradox in birds. *Molecular Biology and Evolution* 1–9. http://academic.oup.com/mbe/article/doi/10.1093/molbev/msx236/4104406/ Avian-genomes-revisited-hidden-genes-uncovered-and.

Boyle EA, Li YI, Pritchard JK. 2017. An Expanded View of Complex Traits: From Polygenic to Omnigenic. *Cell* **169**: 1177–1186. https://www.sciencedirect.com/science/article/pii/S0092867417306293?via{\%}3Dihub.

Brugmann SA, Powder KE, Young NM, Goodnough LH, Hahn SM, James AW, Helms JA, Lovett M. 2010. Comparative gene expression analysis of avian embryonic facial structures reveals new candidates for human craniofacial disorders. *Human molecular genetics* **19**: 920–30. http://www.ncbi.nlm.nih.gov/pubmed/20015954 http://www.pubmedcentral.nih.gov/articlerender.fcgi?artid=PMC2816616.

Brunskill EW, Potter AS, Distasio A, Dexheimer P, Plassard A, Aronow BJ, Potter SS. 2014. A gene expression atlas of early craniofacial development. *Developmental biology* **391**: 133–46.

Butler JE, Kadonaga JT. 2002. The RNA polymerase II core promoter: A key component in the

regulation of gene expression. **16**: 2583–2592.

Capella-Gutierrez S, Silla-Martinez JM, Gabaldon T. 2009. trimAl: a tool for automated alignment trimming in large-scale phylogenetic analyses. *Bioinformatics* **25**: 1972–1973. https://academic.oup.com/bioinformatics/article-lookup/doi/10.1093/bioinformatics/btp348.

Cooney CR, Bright JA, Capp EJR, Chira AM, Hughes EC, Moody CJA, Nouri LO, Varley ZK, Thomas GH. 2017. Mega-evolutionary dynamics of the adaptive radiation of birds. *Nature* **542**: 344–347. http://www.nature.com/doifinder/10.1038/nature21074.

Corcoran P, Gossmann TI, Barton HJ, Consortium TGTH, Slate J, Zeng K. 2017. Determinants of the efficacy of natural selection on coding and noncoding variability in two passerine species. *Genome Biology and Evolution* **10**: 1062–1062. http://academic.oup.com/gbe/article/9/11/2958/4583627 https://academic.oup.com/gbe/article/10/4/1062/4963733.

Ducy P, Desbois C, Boyce B, Pinero G, Story B, Dunstan C, Smith E, Bonadio J, Goldstein S, Gundberg C, et al. 1996. Increased bone formation in osteocalcin-deficient mice. **382**: 448–452.

Felice RN, Goswami A. 2017. Developmental origins of mosaic evolution in the avian cranium. *Proceedings of the National Academy of Sciences* **115**: 201716437. http://www.pnas.org/lookup/doi/10.1073/pnas.1716437115.

Figuet E, Bonneau M, Carrio EM, Nadachowska-brzyska K, Ellegren H, Galtier N. 2017. Life History Traits , Protein Evolution , and the Nearly Neutral Theory in Amniotes. **33**: 1517–1527.

Fisher R a. 1930. The Genetical Theory of Natural Selection. *Genetics* **154**: 272. http://openlibrary.org/books/OL7084333M.

Fletcher W, Yang Z. 2009. INDELible: A Flexible Simulator of Biological Sequence Evolution. *Molecular Biology and Evolution* **26**: 1879–1888. https://academic.oup.com/mbe/article-lookup/doi/10.1093/molbev/msp098.

Foote M. 1997. THE EVOLUTION OF MORPHOLOGICAL DIVERSITY. *Annual Review of Ecology and Systematics* **28**: 129–152. http://linkinghub.elsevier.com/retrieve/pii/0142694X80900496 http://www.annualreviews.org/doi/10.1146/annurev.ecolsys.28.1.129.

Galtier N, Duret L, Glémin S, Ranwez V. 2009. GC-biased gene conversion promotes the fixation of deleterious amino acid changes in primates. **25**: 1–5.

Gossmann TI, Bockwoldt M, Diringer L, Schwarz F, Schumann V-F. 2018. Evidence for Strong Fixation Bias at 4-fold Degenerate Sites Across Genes in the Great Tit Genome. *Frontiers in Ecology and Evolution* **6**: 203. https://www.frontiersin.org/article/10.3389/fevo.2018.00203/full.

Gossmann T, Song B-H, Windsor A, Mitchell-Olds T, Dixon C, Kapralov M, Filatov D, Eyre-Walker A. 2010. Genome wide analyses reveal little evidence for adaptive evolution in many plant species. *Molecular Biology and Evolution* **27**.

Gossmann T, Waxman D, Eyre-Walker A. 2014. Fluctuating selection models and Mcdonald-Kreitman type analyses. *PLoS ONE* **9**.

Grant BR, Grant PR. 1996. High Survival of Darwin ' s Finch Hybrids : Effects of Beak Morphology and Diets. *Ecological Society of America* **77**: 500–509. http://www.jstor.org/stable/2265625.

Grant PR, Grant BR. 2009. The secondary contact phase of allopatric speciation in Darwin's finches. *Proceedings of the National Academy of Sciences* **106**: 20141–20148. http://www.pnas.org/cgi/doi/10.1073/pnas.0911761106.

Gupta S, Stamatoyannopoulos JA, Bailey TL, Noble W. 2007. Quantifying similarity between motifs. *Genome Biology* **8**: R24. http://genomebiology.biomedcentral.com/articles/10.1186/gb-2007-8-2-r24.

Hackett SJ, Kimball RT, Reddy S, Bowie RCK, Braun EL, Braun MJ, Chojnowski JL, Cox WA, Han K-L, Harshman J, et al. 2008. A Phylogenomic Study of Birds Reveals Their Evolutionary History. *Science* **320**: 1763–1768. http://www.sciencemag.org/cgi/doi/10.1126/science.1157704.

Han F, Lamichhaney S, Grant BR, Grant PR, Andersson L, Webster MT. 2017. Gene flow , ancient polymorphism , and ecological adaptation shape the genomic landscape of divergence among Darwin ' s finches. 1–12.

Hill WG. 2010. Understanding and using quantitative genetic variation. *Philosophical Transactions of the Royal Society B: Biological Sciences* **365**: 73–85.

Hu Z, Sackton TB, Edwards SV, Liu JS. 2019. Bayesian Detection of Convergent Rate Changes of Conserved Noncoding Elements on Phylogenetic Trees ed. S.K. Pond. *Molecular Biology and Evolution* **36**: 1086–1100. https://academic.oup.com/mbe/article/36/5/1086/5372678.

Huber SK, Podos J. 2006. Beak morphology and song features covary in a population of Darwin's finches (Geospiza fortis). *Biological Journal of the Linnean Society* **88**: 489–498.

Huerta-Sanchez E, Durrett R, Bustamante CD. 2008. Population genetics of polymorphism and divergence under fluctuating selection. *Genetics* **178**: 325–37. http://www.ncbi.nlm.nih.gov/pubmed/17947441 http://www.pubmedcentral.nih.gov/articlerender.fcgi?artid=PMC2206081.

Hughes M, Gerber S, Wills MA. 2013. Clades reach highest morphological disparity early in their evolution. *Proceedings of the National Academy of Sciences* **110**: 13875–13879. http://www.pnas.org/lookup/doi/10.1073/pnas.1302642110.

Hunter JP. 1998. Key innovations and the ecology of macroevolution. *Trends in ecology & evolution* **13**: 31–6. http://www.ncbi.nlm.nih.gov/pubmed/21238187.

Jones CT, Youssef N, Susko E, Bielawski JP. 2016. Shifting Balance on a Static Mutation–Selection Landscape: A Novel Scenario of Positive Selection. *Molecular Biology and Evolution* **34**: msw237. https://academic.oup.com/mbe/article-lookup/doi/10.1093/molbev/msw237.

Karsenty G, Ferron M. 2012. The contribution of bone to whole-organism physiology. *Nature* **481**: 314–320.

Kimura M. 1983. *The Neutral Theory of Molecular Evolution*. http://books.google.co.il/books?id=olIoSumPevYC{\&}lpg=PP1{\&}dq=the neutral theory of molecular evolution{\%}5Cnhttps://books.google.com/books?hl=en{\&}lr={\&}id=olIoSumPevYC{\&}pgis=1.

Lahti DC, Johnson NA, Ajie BC, Otto SP, Hendry AP, Blumstein DT, Coss RG, Donohue K, Foster SA. 2009. Relaxed selection in the wild. *Trends in Ecology and Evolution* **24**: 487–496.

Lamichhaney S, Berglund J, Almén MS, Maqbool K, Grabherr M, Martinez-Barrio A, Promerová M, Rubin C-J, Wang C, Zamani N, et al. 2015. Evolution of Darwin's finches and their beaks revealed by genome sequencing. *Nature* **518**: 371–375. http://www.nature.com/doifinder/10.1038/nature14181.

Lamichhaney S, Card DC, Grayson P, Tonini JFR, Bravo GA, Näpflin K, Termignoni-Garcia F, Torres C, Burbrink F, Clarke JA, et al. 2019. Integrating natural history collections and comparative genomics to study the genetic architecture of convergent evolution. *Philosophical Transactions of the Royal Society B: Biological Sciences* **374**: 20180248. https://royalsocietypublishing.org/doi/10.1098/rstb.2018.0248.

Lamichhaney S, Han F, Webster MT, Andersson L, Grant BR, Grant PR. 2018. Rapid hybrid speciation in Darwin's finches. *Science* **359**: 224–228. http://www.sciencemag.org/lookup/doi/10.1126/science.aao4593.

Lanfear R, Ho SYW, Love D, Bromham L. 2010. Mutation rate is linked to diversification in birds. **107**: 20423–20428.

Lanfear R, Kokko H, Eyre-walker A. 2014. Population size and the rate of evolution. *Trends in Ecology & Evolution* **29**: 33–41. http://dx.doi.org/10.1016/j.tree.2013.09.009.

Lartillot N. 2013. Interaction between selection and biased gene conversion in mammalian protein-coding sequence evolution revealed by a phylogenetic covariance analysis. *Molecular Biology and Evolution* **30**: 356–368.

Lee NK, Sowa H, Hinoi E, Ferron M, Ahn JD, Confavreux C, Dacquin R, Mee PJ, McKee MD, Jung DY, et al. 2007. Endocrine Regulation of Energy Metabolism by the Skeleton. *Cell* **130**: 456–469.

Lefebvre V, Li P, De Crombrugghe B. 1998. A new long form of Sox5 (L-Sox5), Sox6 and Sox9 are coexpressed in chondrogenesis and cooperatively activate the type II collagen gene. *EMBO Journal* **17**: 5718–5733.

Levy Karin E, Wicke S, Pupko T, Mayrose I. 2017. An Integrated Model of Phenotypic Trait Changes and Site-Specific Sequence Evolution. *Systematic Biology* **66**: 917–933. http://academic.oup.com/sysbio/article/66/6/917/2978030/An-Integrated-Model-of-Phenotypic-Trait-Changes.

Li L, Stoeckert CJJ, Roos DS. 2003. OrthoMCL: Identification of Ortholog Groups for Eukaryotic Genomes. *Genome Research* **13**: 2178–2189. http://genome.cshlp.org/cgi/content/full/13/9/2178.

Lloyd SP. 1982. Least Squares Quantization in PCM. *IEEE Transactions on Information Theory*.

Lowe CB, Clarke JA, Baker AJ, Haussler D, Edwards SV. 2015. Feather Development Genes and Associated Regulatory Innovation Predate the Origin of Dinosauria. *Molecular Biology and Evolution* **32**: 23–28. https://academic.oup.com/mbe/article-lookup/doi/10.1093/molbev/msu309.

Löytynoja A, Goldman N. 2008. Phylogeny-aware gap placement prevents errors in sequence alignment and evolutionary analysis. *Science* **320**: 1632–1635.

Lynch M. 1987. The consequences of fluctuating selection for isozyme polymorphisms in Daphnia. *Genetics* **115**: 657–669.

Machado JP, Johnson WE, Gilbert MTP, Zhang G, Jarvis ED, O'Brien SJ, Antunes A. 2016. Bone-associated gene evolution and the origin of flight in birds. *BMC Genomics* **17**: 1–15. http://dx.doi.org/10.1186/s12864-016-2681-7.

Mallarino R, Grant PR, Grant BR, Herrel A, Kuo WP, Abzhanov A. 2011. Two developmental modules establish 3D beak-shape variation in Darwin's finches. *Proceedings of the National Academy of Sciences* **108**: 4057–4062. http://www.pnas.org/cgi/doi/10.1073/pnas.1011480108.

Manceau M, Domingues VS, Linnen CR, Rosenblum EB, Hoekstra HE. 2010. Convergence in pigmentation at multiple levels: mutations, genes and function. *Philosophical Transactions of the Royal Society B: Biological Sciences* **365**: 2439–2450. https://royalsocietypublishing.org/doi/10.1098/rstb.2010.0104.

Matsumoto T, Akashi H, Yang Z. 2015. Evaluation of Ancestral Sequence Reconstruction Methods to Infer Nonstationary Patterns of Nucleotide Substitution. *Genetics* **200**: 873–90. http://www.genetics.org/lookup/doi/10.1534/genetics.115.177386.

Mayrose I, Otto SP. 2011. A Likelihood Method for Detecting Trait-Dependent Shifts in the Rate of Molecular Evolution. *Molecular Biology and Evolution* **28**: 759–770. https://academic.oup.com/mbe/article-lookup/doi/10.1093/molbev/msq263.

Mcentee JP, Tobias JA, Sheard C, Burleigh JG. 2018. Tempo and timing of ecological trait divergence associated with transitions to coexistence in birds. *Nature Ecology & Evolution* **2**: 1–17.

http://www.biorxiv.org/content/biorxiv/early/2017/04/26/083253.full.pdf.

Mera P, Laue K, Ferron M, Confavreux C, Wei J, Galán-Díez M, Lacampagne A, Mitchell SJ, Mattison JA, Chen Y, et al. 2016. Osteocalcin Signaling in Myofibers Is Necessary and Sufficient for Optimum Adaptation to Exercise. *Cell Metabolism* **23**: 1078–1092.
http://linkinghub.elsevier.com/retrieve/pii/S1550413116302224.

Merkin J, Russell C, Chen P, Burge CB. 2012. Evolutionary Dynamics of Gene and Isoform Regulation in Mammalian Tissues. *Science* **338**: 1593–1599.
http://www.sciencemag.org/cgi/doi/10.1126/science.1228186.

Merrill AE, Eames BF, Weston SJ, Heath T, Schneider RA. 2008. Mesenchyme-dependent BMP signaling directs the timing of mandibular osteogenesis. *Development* **135**: 1223–1234.
http://www.ncbi.nlm.nih.gov/pubmed/18287200
http://www.pubmedcentral.nih.gov/articlerender.fcgi?artid=PMC2844338
http://dev.biologists.org/cgi/doi/10.1242/dev.015933.

Nabholz B, Lanfear R, Fuchs J. 2016. Body mass-corrected molecular rate for bird mitochondrial DNA. *Molecular Ecology* **25**: 4438–4449.

Nabholz B, Uwimana N, Lartillot N. 2013. Reconstructing the phylogenetic history of long-term effective population size and life-history traits using patterns of amino acid replacement in mitochondrial genomes of mammals and birds. *Genome Biology and Evolution* **5**: 1273–1290.

O'Connor TD, Mundy NI. 2013. Evolutionary Modeling of Genotype-Phenotype Associations, and Application to primate coding and Non-coding mtDNA Rate Variation. *Evolutionary Bioinformatics* **9**: EBO.S11600. http://journals.sagepub.com/doi/10.4137/EBO.S11600.

O'Connor TD, Mundy NI. 2009. Genotype–phenotype associations: substitution models to detect evolutionary associations between phenotypic variables and genotypic evolutionary rate. *Bioinformatics* **25**: i94–i100.
https://academic.oup.com/bioinformatics/article-lookup/doi/10.1093/bioinformatics/btp231.

O'Hara RB. 2005. Comparing the effects of genetic drift and fluctuating selection on genotype frequency changes in the scarlet tiger moth. *Proceedings of the Royal Society B: Biological Sciences* **272**: 211–217.

Okita K, Yamanaka S. 2006. Intracellular signaling pathways regulating pluripotency of embryonic stem cells. *Current stem cell research & therapy* **1**: 103–11. http://www.ncbi.nlm.nih.gov/pubmed/18220859.

O'Leary NA, Wright MW, Brister JR, Ciufo S, Haddad D, McVeigh R, Rajput B, Robbertse B, Smith-White B, Ako-Adjei D, et al. 2016. Reference sequence (RefSeq) database at NCBI: current status, taxonomic expansion, and functional annotation. *Nucleic Acids Research* **44**: D733–D745.
https://academic.oup.com/nar/article-lookup/doi/10.1093/nar/gkv1189.

Östlund G, Schmitt T, Forslund K, Köstler T, Messina DN, Roopra S, Frings O, Sonnhammer EL. 2009. Inparanoid 7: New algorithms and tools for eukaryotic orthology analysis. *Nucleic Acids Research* **38**: 196–203.

Parsons KJ, Albertson RC. 2009. Roles for Bmp4 and CaM1 in Shaping the Jaw: Evo-Devo and Beyond. *Annual Review of Genetics* **43**: 369–388.
http://www.annualreviews.org/doi/10.1146/annurev-genet-102808-114917.

Piechota M, Korostynski M, Przewlocki R. 2010. Identification of cis-Regulatory Elements in the Mammalian Genome: The cREMaG Database ed. C.A. Ouzounis. *PLoS ONE* **5**: e12465.
https://dx.plos.org/10.1371/journal.pone.0012465.

Podos J. 2001. Correlated evolution of morphology and vocal structure in Darwin's finches. *Nature* **409**: 185–188.

Prudent X, Parra G, Schwede P, Roscito JG, Hiller M. 2016. Controlling for Phylogenetic Relatedness and Evolutionary Rates Improves the Discovery of Associations Between Species' Phenotypic and Genomic Differences. *Molecular Biology and Evolution* **33**: 2135–2150. https://academic.oup.com/mbe/article-lookup/doi/10.1093/molbev/msw098.

Prum RO, Berv JS, Dornburg A, Field DJ, Townsend JP, Lemmon EM, Lemmon AR. 2015. A comprehensive phylogeny of birds (Aves) using targeted next-generation DNA sequencing. *Nature* **526**: 569–573. http://www.nature.com/doifinder/10.1038/nature15697.

Raymond MH, Schutte BC, Torner JC, Burns TL WM. 1999. Osteocalcin: genetic and physical mapping of the human gene BGLAP and its potential role in postmenopausal osteoporosis. *Genomics* **60**: 210–17.

R Core Team. 2018. *R: A Language and Environment for Statistical Computing*. R Foundation for Statistical Computing, Vienna, Austria https://www.r-project.org/.

Revell LJ. 2012. phytools: An R package for phylogenetic comparative biology (and other things). *Methods in Ecology and Evolution*.

Ricklefs RE. 2004. Cladogenesis and morphological diversification in passerine birds. *Nature*.

Rockman MV. 2012. The QTN program and the alleles that matter for evolution: All that's gold does not glitter. *Evolution* **66**: 1–17.

Rosenblum EB, Parent CE, Brandt EE. 2014. The Molecular Basis of Phenotypic Convergence. *Annual Review of Ecology, Evolution, and Systematics* **45**: 203–226. http://www.annualreviews.org/doi/10.1146/annurev-ecolsys-120213-091851.

Sackton TB, Grayson P, Cloutier A, Hu Z, Liu JS, Wheeler NE, Gardner PP, Clarke JA, Baker AJ, Clamp M, et al. 2019. Convergent regulatory evolution and loss of flight in paleognathous birds. *Science (New York, NY)* **364**: 74–78. http://www.ncbi.nlm.nih.gov/pubmed/30948549.

Schluter D. 2000. The Ecology of Adaptive Radiation.

Seki R, Li C, Fang Q, Hayashi S, Egawa S, Hu J, Xu L, Pan H, Kondo M, Sato T, et al. 2017. Functional roles of Aves class-specific cis-regulatory elements on macroevolution of bird-specific features. *Nature Communications* **8**: 14229. http://www.nature.com/doifinder/10.1038/ncomms14229.

Sharma V, Hecker N, Roscito JG, Foerster L, Langer BE, Hiller M. 2018. A genomics approach reveals insights into the importance of gene losses for mammalian adaptations. *Nature Communications* **9**: 1215. http://www.nature.com/articles/s41467-018-03667-1.

Shultz AJ, Sackton TB. 2019. Immune genes are hotspots of shared positive selection across birds and mammals. *eLife* **8**.

Simpson GG. 1944. *Tempo and mode in evolution.* Columbia Univ. Press, New York https://www.worldcat.org/title/tempo-and-mode-in-evolution/oclc/993515.

Stern DL. 2013. The genetic causes of convergent evolution. *Nature Reviews Genetics* **14**: 751–764. http://www.nature.com/articles/nrg3483.

Stroud JT, Losos JB. 2016. Ecological Opportunity and Adaptive Radiation. *Annual Review of Ecology, Evolution, and Systematics* **47**: 507–532. http://www.annualreviews.org/doi/10.1146/annurev-ecolsys-121415-032254.

Szklarczyk D, Franceschini A, Wyder S, Forslund K, Heller D, Huerta-Cepas J, Simonovic M, Roth A,

Santos A, Tsafou KP, et al. 2015. STRING v10: Protein-protein interaction networks, integrated over the tree of life. *Nucleic Acids Research* **43**: D447–D452.

Venditti C, Meade A, Pagel M. 2011. Multiple routes to mammalian diversity. *Nature* **479**: 393–396. http://dx.doi.org/10.1038/nature10516.

Wang J, Vasaikar S, Shi Z, Greer M, Zhang B. 2017. WebGestalt 2017: a more comprehensive, powerful, flexible and interactive gene set enrichment analysis toolkit. *Nucleic Acids Research* **45**: W130–W137. https://academic.oup.com/nar/article-lookup/doi/10.1093/nar/gkx356.

Watterson G. 1975. On the number of segregating sites in genetical models without recombination. *Theoretical Population Biology* **7**: 256–276. https://www.sciencedirect.com/science/article/pii/0040580975900209?via{\%}3Dihub.

Weber CC, Nabholz B, Romiguier J, Ellegren H. 2014. Kr/Kc but not dN/dS correlates positively with body mass in birds, raising implications for inferring lineage-specific selection. 1–13.

Weir BS, Cockerham CC. 1984. Estimating F-Statistics for the Analysis of Population Structure. *Evolution* **38**: 1358. https://www.jstor.org/stable/2408641?origin=crossref.

Whitney O, Pfenning AR, Howard JT, Blatti CA, Liu F, Ward JM, Wang R, Audet J-N, Kellis M, Mukherjee S, et al. 2014. Core and region-enriched networks of behaviorally regulated genes and the singing genome. *Science* **346**: 1256780–1256780. http://www.sciencemag.org/cgi/doi/10.1126/science.1256780.

Wilkinson L. 2011. ggplot2: Elegant Graphics for Data Analysis by WICKHAM, H. *Biometrics*.

Wirthlin M, Lovell PV, Jarvis ED, Mello CV. 2014. Comparative genomics reveals molecular features unique to the songbird lineage. *BMC Genomics* **15**: 1082. http://bmcgenomics.biomedcentral.com/articles/10.1186/1471-2164-15-1082.

Wittkopp PJ, Kalay G. 2012. Cis-regulatory elements: Molecular mechanisms and evolutionary processes underlying divergence. **13**: 59–69.

Wright D, Boije H, Meadows JRS, Bed'hom B, Gourichon D, Vieaud A, Tixier-Boichard M, Rubin C-J, Imsland F, Hallböök F, et al. 2009. Copy Number Variation in Intron 1 of SOX5 Causes the Pea-comb Phenotype in Chickens ed. D.L. Stern. *PLoS Genetics* **5**: e1000512. http://dx.plos.org/10.1371/journal.pgen.1000512.

Wu P, Jiang T-X, Suksaweang S, Widelitz RB, Chuong C-M. 2004. Molecular shaping of the beak. *Science (New York, NY)* **305**: 1465–6. http://www.ncbi.nlm.nih.gov/pubmed/15353803 http://www.pubmedcentral.nih.gov/articlerender.fcgi?artid=PMC4380220.

Xu X, Zhou Z, Dudley R, MacKem S, Chuong CM, Erickson GM, Varricchio DJ. 2014. An integrative approach to understanding bird origins. *Science* **346**.

Yang Z. 1998. Likelihood ratio tests for detecting positive selection and application to primate lysozyme evolution. *Molecular Biology and Evolution* **15**: 568–573. https://academic.oup.com/mbe/article-lookup/doi/10.1093/oxfordjournals.molbev.a025957.

Yang Z. 2007. PAML 4: Phylogenetic analysis by maximum likelihood. *Molecular Biology and Evolution* **24**: 1586–1591.

Yang Z, Nielsen R. 1998. Synonymous and nonsynonymous rate variation in nuclear genes of mammals. *Journal of Molecular Evolution* **46**: 409–418.

Yang Z, Nielsen R, Hasegawa M. 1998. Models of Amino Acid Substitution and Applications to Mitochondrial Protein Evolution. *Mol Biol Evol* **15**: 1600–1611.

Figure Legends

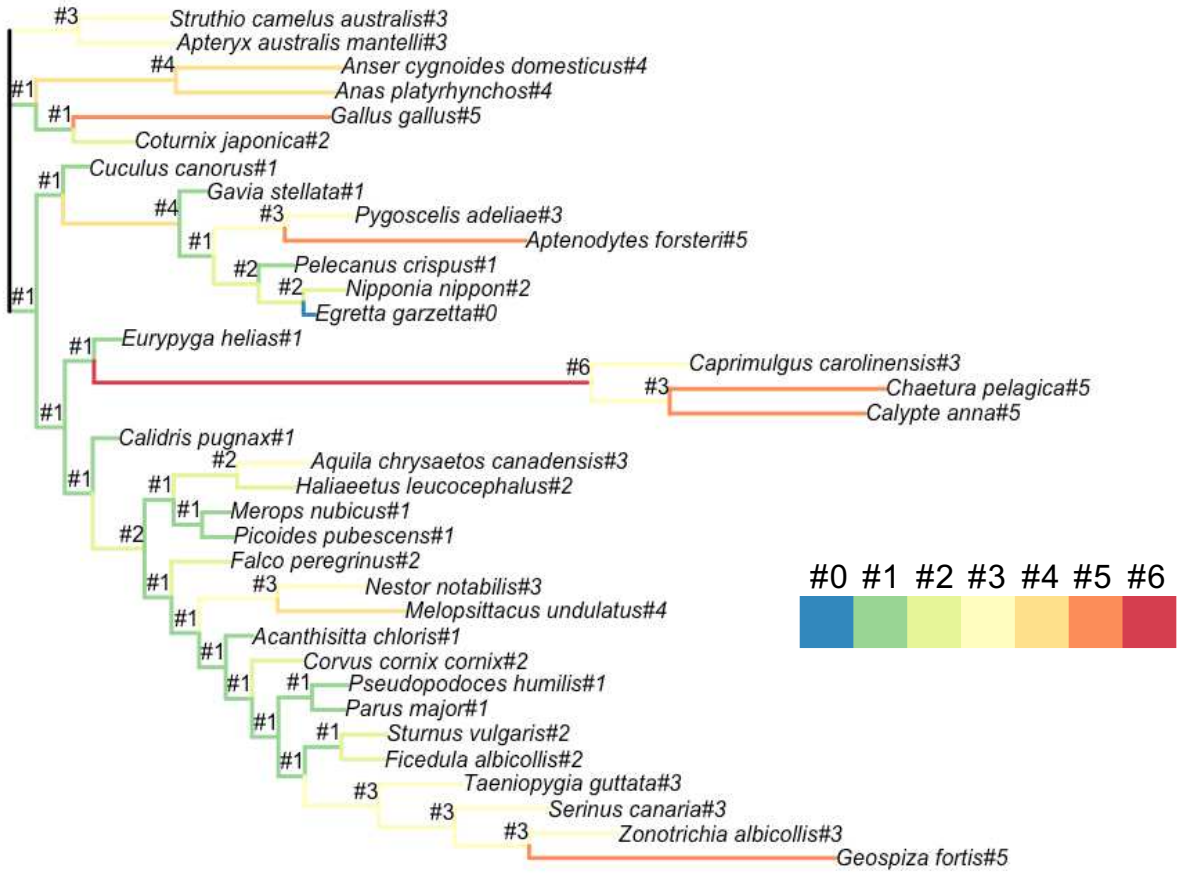

Figure 1: **An example tree illustrating the grouping of branches according their beak shape morphological rates.** The marked topology was then used as input for branch model in PAML (codeml for coding DNA and baseml for noncoding DNA). The maximum number of bins is eight for the coding gene set and 16 for the avian-specific highly conserved elements (ASHCE) set. Here, as an example, a binning with seven bins (#0 to #6) is shown.

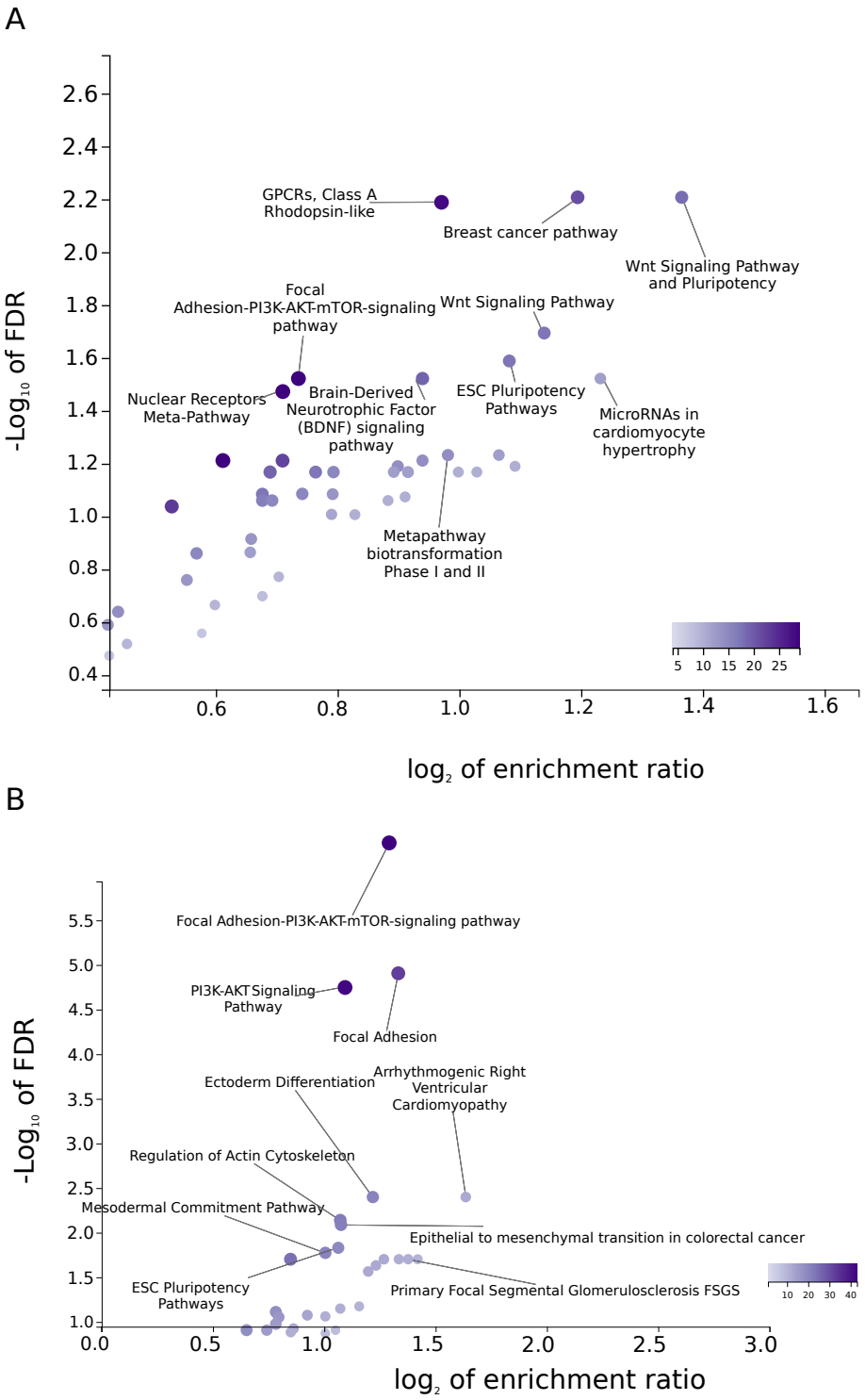

Figure 2: **Pathway enrichment analysis of (A) 1,434 protein coding genes and (B) 848 genes nearby avian conserved genomic regions** that show heterogeneity of substitution rates across branches that are grouped according to their beak shape morphological change rates. False discovery rate (FDR) and enrichment ratio stem from the pathway enrichment analysis in WebGestalt (Wang et al. 2017) using all analysed genes and human annotations, as these are the most comprehensive annotation databases to date. The color of the dots is denoted in the color scale and proportional to the category size, as definded by WebGestalt.

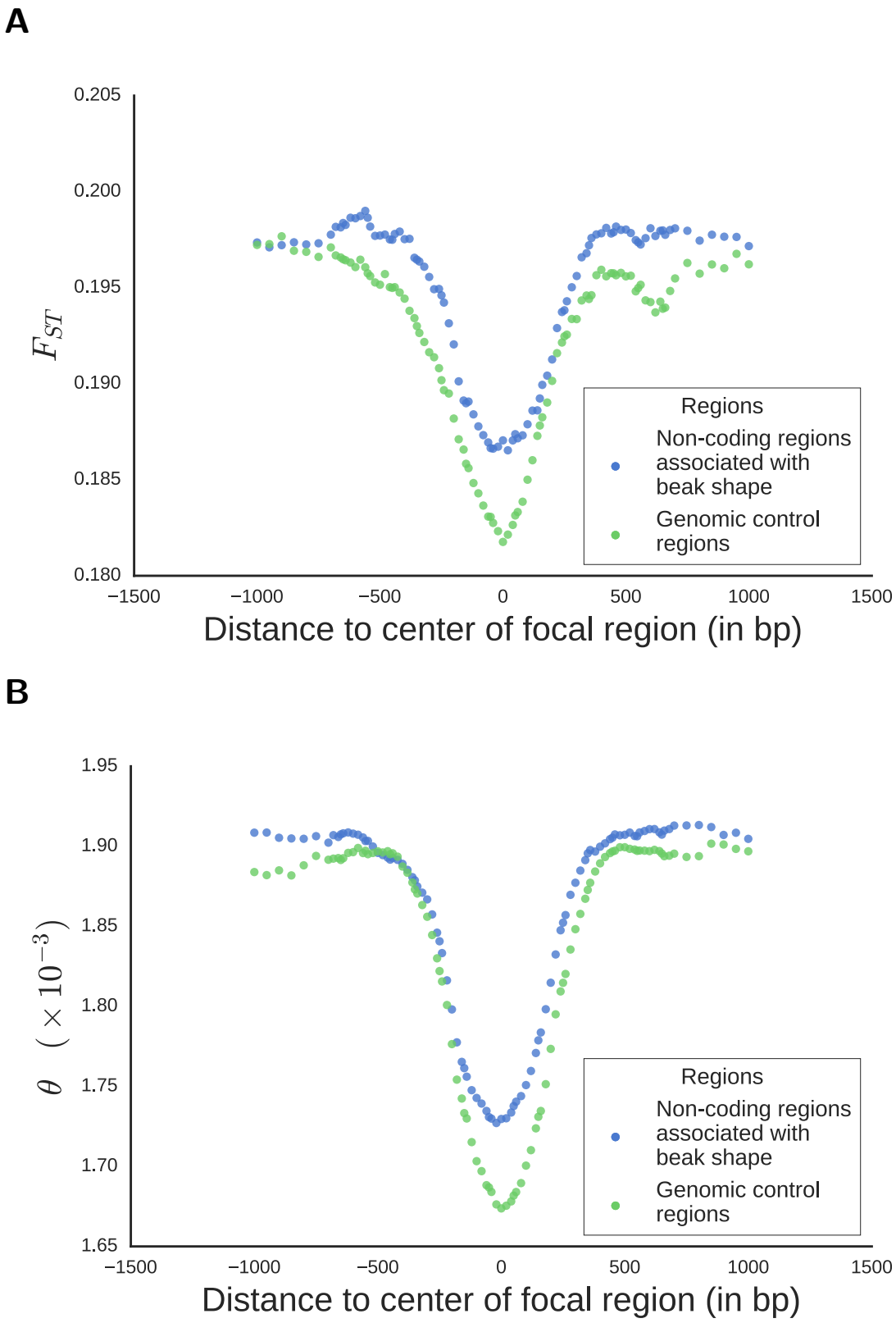

Figure 3: **Identified noncoding genomic regions in a microevolutionary context in populations of Darwin's finches.** (A) Measures for genetic differentiation among populations, F_{ST}, show contrasting genetic diversity in Darwin finch populations with blunt and pointy beaks, respectively. The identified loci associated with beak shape evolution over macroevolutionary time and nearby regions show a stronger differentiation relative to similar loci that are not asscoatiated with beak shape. (B) Total genetic diversity is higher for beak shape associated loci and nearby regions.

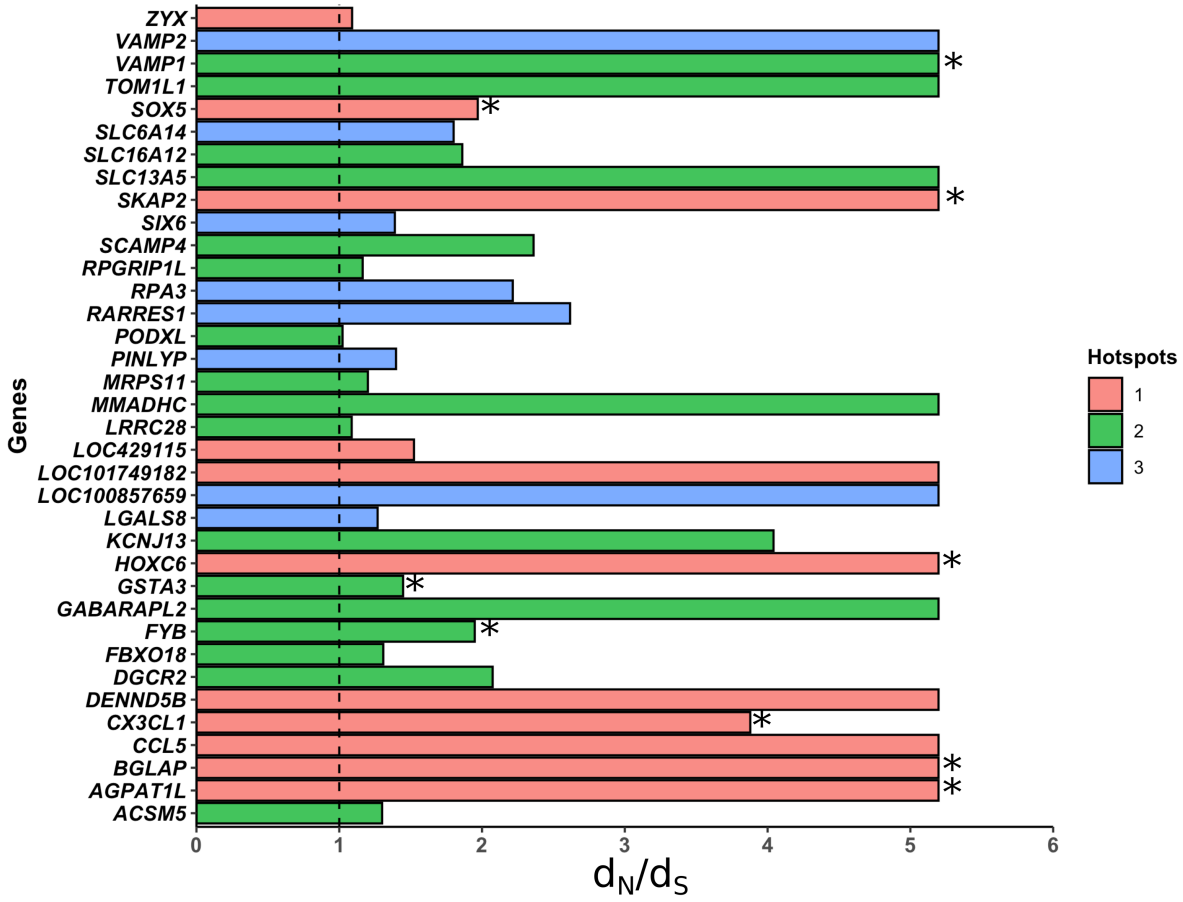

Figure 4: **Elevated rates of protein evolution (d_N/d_S) associated with hotspots of beak shape morphological diversification**. Shown are d_N/d_S values for selected hotspot branches for 36 genes detected with d_N/d_S>1. Black dotted line formally indicates neutrality (d_N/d_S = 1) and asteriks indicate genes for which the branch-specific estimate d_N/d_S is significantly different from 1 (e.g. indicative of positive selection). Hotspots 1, 2 and 3 refer to the branches of the tree with the fastest, 2nd fastest and 3rd fastest rates of beak shape morphological change, respectively (Figure S3). For visualisation purposes are large d_N/d_S values truncated at 5.2 (the estimate for SKAP2).

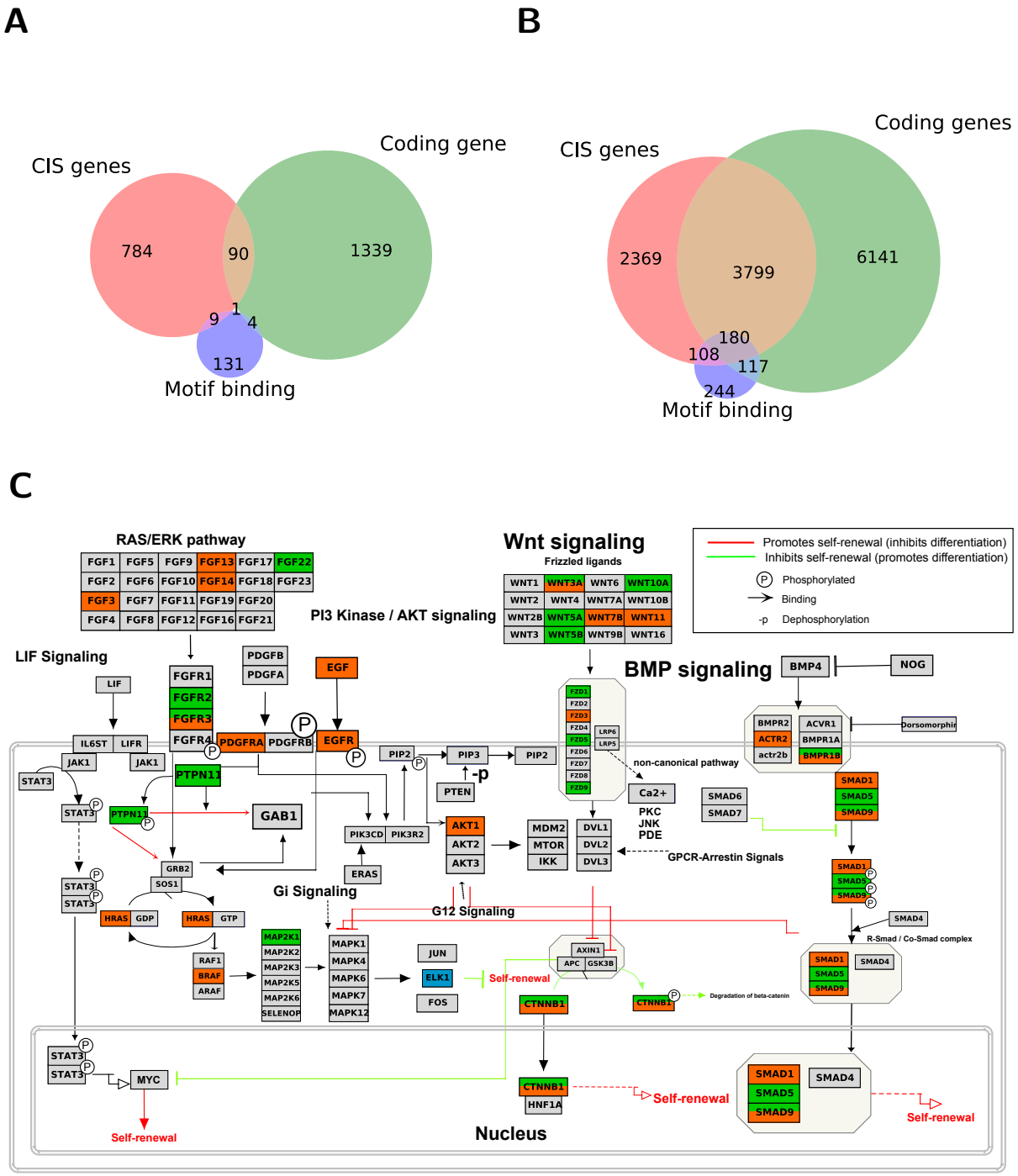

Figure 5: **Comparison of beak shape associated gene sets derived from coding and noncoding genomic regions.** (A) Overlap of the identified gene sets (B) Overlap of genes included in each dataset (background) (C) 32 Genes identified in our study occurring in the ESC pluripotent pathways, including BMP and Wnt signalling. Genes highlighted in green were detected in the protein coding analysis, while genes highlighted in orange were detected in the noncoding analysis. ELK1, labelled in blue, was detected as one of the transcription motif binding proteins. Coding genes denote all genes analysed for the protein coding gene analysis, CIS genes are genes in local proximity to analysed noncoding genomic regions, Motif binding are annotated proteins from the motif binding identification with TOMTOM (Gupta et al. 2007).

Tables

Table 1: **Top phenotype ontology associations identified from the identified genomic loci**, coding genes, genes nearby noncoding regions and possible DNA binding proteins. * marked ontology terms are based on disease annotation database approach (GLAD4U).

Human Phenotype ID	Description	Set size	Expected	Ratio	P-value
Coding gene set (1,434 genes)					
HP:0100585	Telangiectasia of the skin	40	6.1374	2.4440	0.00046
HP:0001651	Dextrocardia	47	7.2114	2.3574	0.00032
HP:0031654	Abnormal pulmonary valve physiology	59	9.0526	2.2093	0.00027
HP:0100242	Sarcoma	65	9.9732	2.1056	0.00040
HP:0000987	Atypical scarring of skin	73	11.2010	2.0534	0.00032
HP:0010766	Ectopic calcification	108	16.5710	1.8104	0.00049
HP:0000238	Hydrocephalus	157	24.0890	1.6605	0.00043
Non-coding gene set					
(884 genes nearby non-coding regions)					
HP:0011338	Abnormality of mouth shape	59	10.1430	1.7746	0.00736
HP:0010766	Ectopic calcification	73	12.5500	1.6733	0.00824
HP:0100242	Sarcoma	53	9.1115	1.6463	0.02801
HP:0001417	X-linked inheritance	92	15.8160	1.6439	0.00439
HP:0010576	Intracranial cystic lesion	57	9.7992	1.6328	0.02547
HP:0000204	Cleft upper lip	61	10.4870	1.6211	0.02313
HP:0000662	Nyctalopia	59	10.1430	1.5774	0.03478
HP:0000422	Abnormality of the nasal bridge	283	48.6520	1.2538	0.02098
Motif binding proteins (145 genes)					
*PA443736**	Cleft Lip	33	3.9165	2.5533	0.00260
*PA446836**	Craniofacial Abnormalities	51	6.0527	2.3130	0.00094
*PA443223**	Congenital Abnormalities	87	10.3250	2.0338	0.00023
HP:0000159	Abnormal lip morphology	65	11.7620	1.4453	0.03522

Table 2: **Enrichment test for proteins identified as d_N/d_S heterogeneous/homogeneous and interaction partners of BMP4/ALX1/CALM1**. d_N/d_S values were retrieved for groups of branches with similar beak shape morphological rates. The common interactome of BMP4/ALX1/CALM1 consists of 467 proteins, of which 256 were included in our gene analysis. Altogether, we identified 53 proteins of the BMP4/ALX1/CALM1 interactome that showed significant variation in their d_N/d_S values (heterogeneous d_N/d_S).

Protein category	d_N/d_S heterogeneity	d_N/d_S homogeneous	Ratio
BMP4/ALX1/CALM1 and interaction partners	53	203	0.26
Other proteins	1381	8601	0.16
P-value (χ^2 2×2 test, df=1)			**0.002**

Table 3: **Enrichment tests for genes nearby genomic regions that show significant hetereogeneity in their substitution rates (heterogeneity was tested for grouped branches according to beak shape morphological change rates) versus a set of 511 known genes involved in craniofacial development in mice**. Gene sets were further subset according to whether their was a significant correlation between morphological change of beak shape and substitution rates. P-values were obtained using a χ^2 2×2 test.

Gene category	Subset	Total	In craniofacial gene set	not in craniofacial gene set	Ratio
Genes near identified genomic regions		884	48	836	0.057^{*}
	Positively correlated	163	17	146	0.116^{***}
	Not positively correlated	721	31	690	$0.045^{n.s.}$
Genes near non-identified genomic regions		5572	201	5371	0.037

Supplemental Material

Supplemental Methods

Multiple sequence alignments for protein coding genes

We used genomes of 57 bird species with high quality annotations from NCBI RefSeq (O'Leary et al. 2016) (Table S2). First, 12,013 orthologous protein coding genes were retrieved using RefSeq and HGNC gene identifiers, alongside reciprocal BLAST approaches based on three focal species, chicken, great tit and zebra finch - three of the best annotated high quality bird genomes available to date (Li et al. 2003; Östlund et al. 2009; Afanasyeva et al. 2018). We then performed a first set of alignment runs using PRANK (Löytynoja and Goldman 2008). To ensure the quality of these sequence alignments, we applied a customised pipeline. Firstly, alignments were filtered for length and the number of species they contained. Generally, we applied a length filter that removed alignments containing more than 1500 amino acid residues (for computational reasons) and less than 50 amino acid residues (for power reasons). These thresholds were based on distributions of overall sequence length across all alignments. Furthermore, we compared the number of gaps and length of sequences to a reference sequence in all alignments. Regarded as the most well-annotated, high-quality avian genome, we selected the red jungle fowl (i.e. chicken, *Gallus gallus*) as our reference sequence for all alignments (Hillier et al. 2004; Warren et al. 2017). Sequences determined to be too dissimilar (e.g. because of falsely aligning non-homologous regions within a protein), based on gappyness – the amount of gaps in a sequence – and overall sequence length, relative to our reference species sequence, were also removed from alignments. Specifically, for gappyness, if gaps resulted in more than 20% dissimilarity with our reference sequence, sequences

were removed. We also limited the analyses to alignments containing 20 or more species, and removed alignments that did not contain the reference chicken sequence.

For reliable estimation of sequence divergence at the protein level, sequences that appeared too divergent were removed - caused by either elevated local mutation rate or, more likely, by falsely assigned orthologies. For this pairwise estimation of d_N, d_S and d_N/d_S was performed to determine saturation of non-synonymous and synonymous substitutions. Removal of saturated sequences was accomplished in two ways. First, pairwise synonymous substitution rates deemed too large were removed (d_S>5), and second, if synonymous substitution rates exceeded twice the pairwise synonymous substitution rate between *G. gallus* and *Taeniopygia guttata* (zebra finch), two of our focal species, sequences were removed. In addition, if the pairwise non-synonymous substitution rate, d_N, and the non-synonymous to synonymous substitution rate, d_N/d_S, exceeded two (d_N>2 and d_N/d_S>2) sequences were removed from alignments. By this the sequences are conservatively aligned which reduces the chances of alignment-error signal of (positive) selection.

After a second alignment step with PRANK, to ensure positional homology, we utilised two masking programs: GBLOCKS and ZORRO. GBLOCKS calculates and uses positional homology to determine contiguous segments that are not conserved (Talavera and Castresana 2007). Additionally, GBLOCKS accounts for rapidly-evolving, homologous positions and flanking positional homology. For this, we used the following parameters to identify and remove unreliable positions: -t=p, -k=y, n=y, v =32000, -p=t. To supplement this, we used ZORRO, a probabilistic masking program which calculates posterior probabilities to determine the reliability of positions (Wu et al. 2012). Posterior probabilities calculated by ZORRO translate into scores that range from 0 to 10 – the higher the score, the better the positional homology. Positions that scored below 9 were removed from sequences. The removal of unreliable positions from sequences was performed with PAL2NAL (Suyama et al. 2006) using a customised script. Equally, PAL2NAL generated for each protein alignment the corresponding codon alignment in preparation for evolutionary analyses. A final length filter was applied to remove any alignments with a sequence length below 50 amino acids.

Rates of morphological beak shape evolution

Information on beak shape evolution was extracted from a recent study (Cooney et al. 2017) that quantified patterns of beak shape evolution across 2,028 species (>97% extant avian genera) covering the entire breadth of the avian clade. Briefly, this study used geometric morphometric data based on 3-D scans of museum specimens and multivariate rate heterogeneous models of trait evolution (Venditti et al. 2011) to estimate rates of beak shape evolution for all major branches in the avian phylogeny. Importantly, the beak shape measurements derived from this study are independent of variation in beak size, the effects of which are removed as part of standard geometric morphometric analyses (see Cooney et al. (2017) for full details). This is useful for our purposes as beak size tends to be strongly related to body size (which is known to covary with several genetic parameters), and because beak shape (rather than size) represents a key axis of ecomorphological differentiation between major avian groups (Cooney et al. 2017). To extract rate estimates for the species included in this study, we first pruned the 2,028 tip morphology rate-scaled phylogenies derived from Cooney et al. (2017) (based on the Hackett et al. (Hackett et al. 2008) backbone) to include only species for which coding/genomic information was available. We then divided the branch lengths in this pruned morphology rate-scaled tree by time (i.e. branch lengths from a similarly pruned time tree, also derived from Cooney et al. (2017)), to generate rate estimates specific to each branch in the pruned subtree. It is worth noting that our approach of pruning the

2,028 tip morphology rate-scaled tree is preferable to running a separate rates analysis including only a limited number of species included in our genomic dataset because the increased density of sampling in the larger tree will permit more accurate estimation of the magnitude and phylogenetic position of rate shifts in beak shape evolution across branches of the phylogeny.

Binned branch approach for the detection of large-effect genes and regulatory regions

To detect genes that may be undergoing repeated periods of rapid, possibly adaptive, evolution across multiple lineages, we grouped branches in each alignment phylogeny according to their rates of morphological evolution using *k*-means binning (Lloyd 1982). Here, we opted for up to eight (coding) and 16 (ASCHE) bins, respectively, to enable robust statistical analysis but still reasonable computational time for the substitution rate analysis. To phylogenetically link the genetic data to the morphological data we relied on the Hackett et al. backbone (Hackett et al. 2008), hence we did not account for phylogenetic heterogeneity among genes and possible gene-tree species tree discordance. Branches were grouped incrementally based on rates of trait evolution using a *k*-means binning approach, with the first bin representing branches with the slowest rates of morphological evolution, and the last bin representing branches with the fastest rates of morphological evolution (Figure 1). We assumed that genes involved in beak shape evolution would experience evolutionary rate change at the protein level ($d_{\mathrm{N}}/d_{\mathrm{S}}$) proportional to their respective rate of morphological evolution. Theoretically, we hypothesize that genes important in beak shape evolution across many branches would show a strong positive correlation.

In our analysis, we tested this using a branch model which assumes different substitution rates ($d_{\mathrm{N}}/d_{\mathrm{S}}$) across different, pre-defined, branches in a phylogeny using codeml (Yang 2007). Critically, the branch model may be useful in the detection of adaptive evolution occurring on particular branches (Yang et al. 1998; Yang 1998). Furthermore, we selected the branch model due to computational efficiency; the branch-site model and free-ratio model was deemed computationally intractable for a phylogeny of up to 57 species. Branches in each alignment's phylogeny were marked according to their respective bins (typically ranging from 1 to 8). Labelling bins as distinct types of branches allowed for the estimation of up to eight different $d_{\mathrm{N}}/d_{\mathrm{S}}$ values per gene. Conjointly, for each binned model, an alternative null model assuming no difference in $d_{\mathrm{N}}/d_{\mathrm{S}}$ between branches was run (one-ratio model). The difference between models was compared using a likelihood-ratio test (LRT) by comparing twice the log-likelihood difference between the two models which is assumed to be χ^2 distributed, with the relevant degrees of freedom (Yang 2007) (e.g, seven degrees of freedom in case eight different branch categories were classified). If the binned model showed a significant difference to the one-ratio model an association between beak shape change and molecular rate change was inferred.

To estimate rate heterogeneity among branches in noncoding regions, we used a model where we assumed equal rates among branches (e.g. a global clock, clock=1) and compared it to a model where we assumed different rates for the binned branches (clock=2), assessing significant differences between the models using a likelihood ratio test using baseml from the paml package (Yang 2007). For the simulations (Figure S2) we randomly chose a 222bp long genomic region with 67 species. We run a free branch model (clock=0) and used the obtained parameters as input for INDELible (Fletcher and Yang 2009). We simulated 100 sets of sequences and applied two types of binning: (1) A binning that grouped similar branch lengths and (2) an arbitrary binning. We considered 5 different numbers of bins (with 2,4,8,16 and unrestricted number of bins). We then conducted rate estimation on each of the binning approaches and calculated how well these

estimates correlated (Kendall's τ correlation coefficient) with the input parameters for INDELible (e.g. the simulation input) as well as the estimated values from the free branch model.

Hotspot approach for the detection of genes under positive selection

For each alignment we generated and conducted three independent branch models, corresponding to the three most rapidly evolving branches in each phylogeny. A null model assuming no differences in $d_{\mathrm{N}}/d_{\mathrm{S}}$ across branches in the phylogeny was conjointly computed. Again, the LRT was calculated to determine whether differences between each 'hotspot' model and the null model were significant. It is important to note that branches are not uniformly selected across alignments and alignment trees. This is because alignments vary in the number of species and branches they contain due to the filtering process applied. Hence, the selection of branches is dependent on species rates of morphological evolution relative to other species – the exclusion of species, particularly rapidly-evolving branches, causes new branches to be recruited in the hotspot-branch model. In total, five different branches rotate over our three hotspots (Figure S3). This can be done because each analysis is conducted per gene on the correctly pruned phylogeny. In most cases our fastest branch was an internal branch leading to the diversification of swifts (Apodidae), nightjars and their allies, (Caprimulgidae) and hummingbirds (Trochilidae). This is plausible given the disparity in beak shape, physiology and ecology that has arisen in this clade (Prum et al. 2015; Cooney et al. 2017).

Phenotype and pathway ontologies, protein databases and statistical analyses

To determine the putative function of genes detected and enriched according to pathway and phenotype enrichment, we used WebGestalt (Wang et al. 2017) based on the human annotation. Specifically, we used the latest release of WebGestalt (last accessed 11.3.2019), and ran an Overrepresentation Enrichment Analysis (ORA) for phenotypes (Human Phenotype Ontology), pathways (Wikipathways) and diseases (Glad4U). We set the minimum number of genes for a category to 40 and reported top statistical significant results as weighted cover set (as implemented in WebGestalt). We also obtained a set of 511 genes known from mouse knock-out phenotypes to result in abnormal craniofacial morphology or development (Brunskill et al. 2014). To account for multiple testing in our binned and hotspot models, χ^2-squared P-values were corrected using the Benjamini-Hochberg procedure (Benjamini and Hochberg 1995). We used Kendall's τ correlation coefficient to compare the association between increasing bin number and corresponding $d_{\mathrm{N}}/d_{\mathrm{S}}$ (coding) and substitution rates (noncoding) for each gene. Statistical analysis was conducted using the SciPy library in Python, and graphs were produced using the 'tidyverse' package in R (Wilkinson 2011; R Core Team 2018) and the 'matplotlib' package in Python. Phylogenies were produced using the 'phytools' package in R (Revell 2012). Protein interaction partners for ALX1, BMP1 and CALM1 were retrieved from the STRING database (Szklarczyk et al. 2015) based on the human annotation requiring a minimum confidence score of 0.6 for all interaction partners. Motif detection was conducted using DREME (Bailey 2011) along with the identification of potential binding proteins using TOMTOM (Gupta et al. 2007). Specifically, we focused on vertebrate binding proteins using a common set of three available databases (JASPAR2018_CORE_vertebrates_non-redundant, jolma2013, uniprobe_mouse) that together contained 649 annotated motif binding proteins.

Population genetic analysis in Darwin's finches population with diverse beak morphology

We used the 39,806 noncoding genomic loci as focal regions and 1000 bp on either site of their center. To map our identified genomic loci onto the medium ground finch (*Geospiza fortis*) reference genome (Zhang et al. 2014), we used the best BLAST (default parameters) hit per region. We also extracted the same number of size and chromosome matched genomic regions that did not show an association with beak shape morphological diversification as control regions. To study the effect of selection at the focal and nearby sites due to linkage, a sliding window approach was used, applying a window size of 400bp every 50 bp around the center of the focal regions (Other window and step sizes gave very similar results). For F_{ST} we used the highest per site F_{ST} value for a particular genomic region in a given window and calculated the mean across all regions. Watterson's θ was calculated per genomic region in a given window and then averaged across all loci.

Supplemental Figures

Supplemental Figure S1

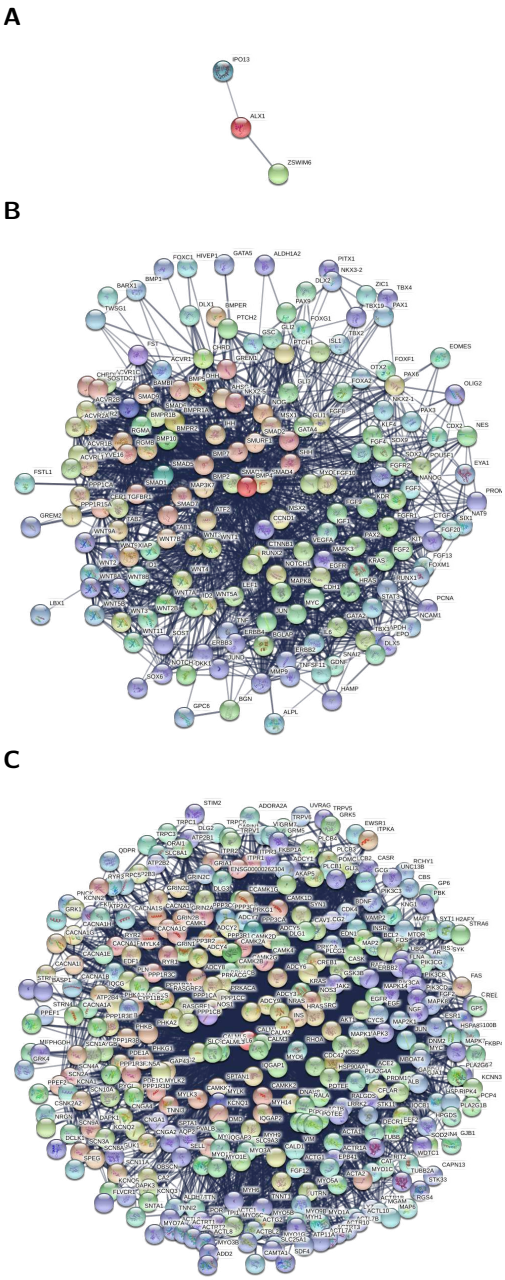

Figure S1: ***In-silico* interaction networks derived from the STRING database** for three proteins previously shown to be involed in the development of beak shape morphology.

Supplemental Figure S2

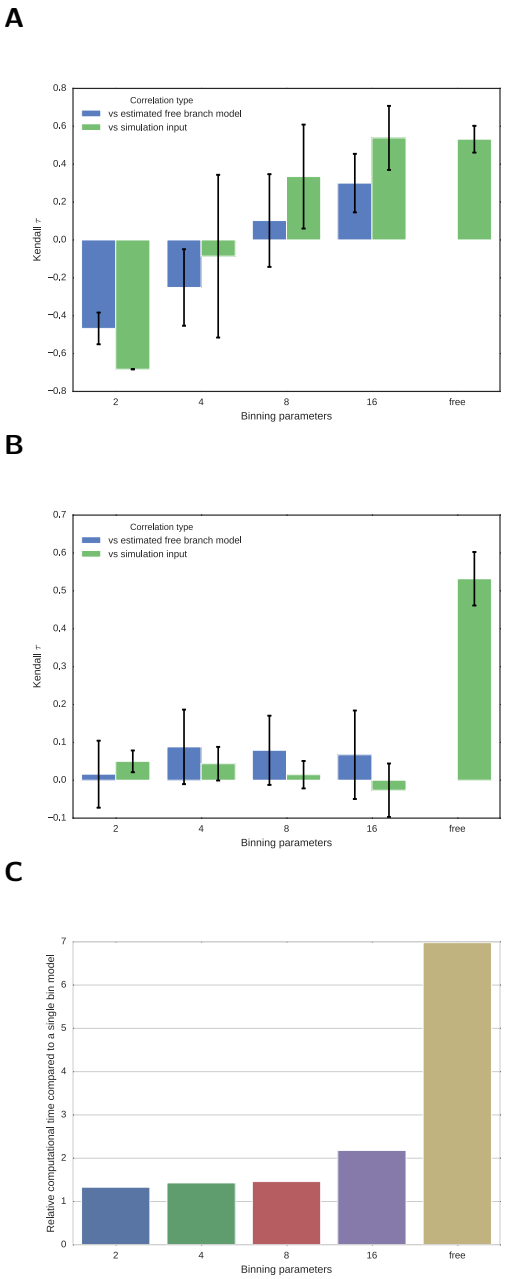

Figure S2: **Simulations to capture rate hetereogenity among branches by co-estimating rates of molecular change for grouped branches, estimated for noncoding regions.** (A) Correlation coefficients (Kendall τ) of simulated and estimated rate hetereogeneity for different bin numbers, where branches of similar rates are grouped together. (B) Same approach using an arbitrary binning of branches (C) Relative computational time requirements for different number of bins.

Supplemental Figure S3

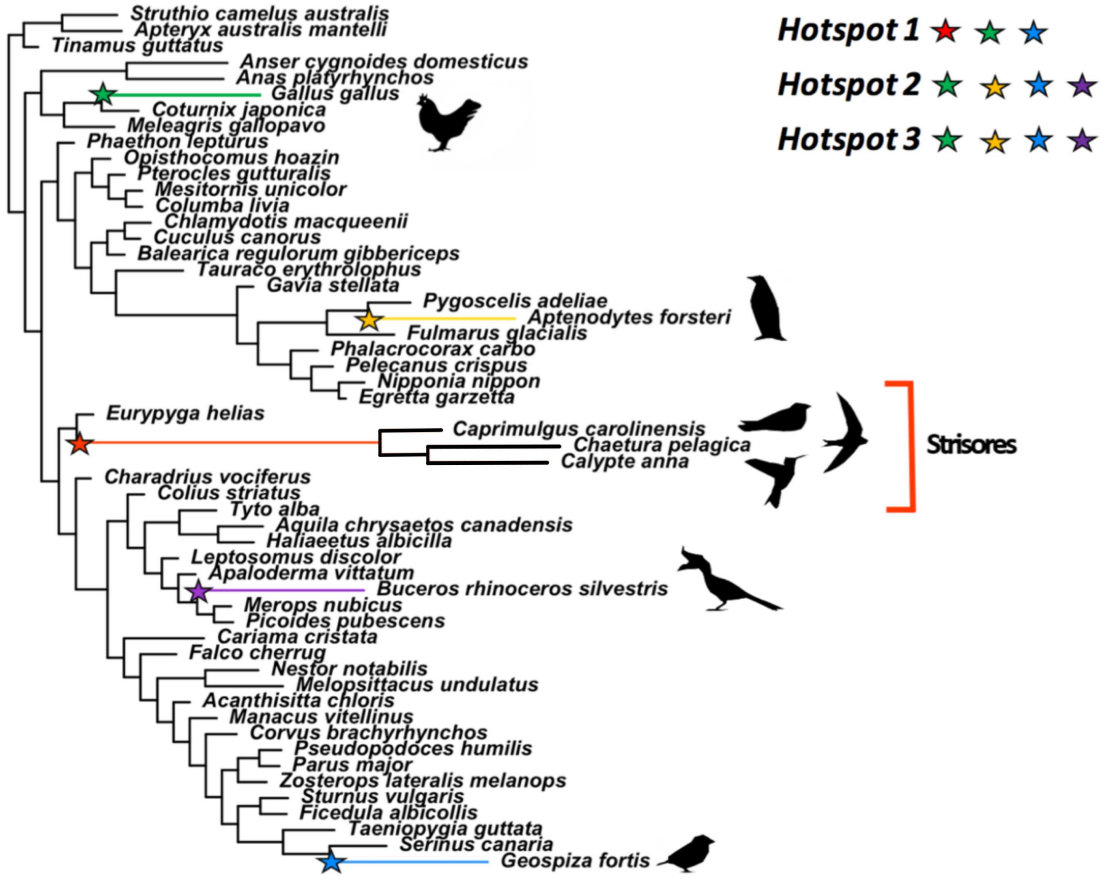

Figure S3: **An illustration of the hotspot approach containing phylogeny and the five fastest rapidly-evolving branches selected for hotspot model.** For the phylogeny, branch lengths correspond to the scaled rate of morphological beak shape evolution. Branches coloured and indicated with a star are rapidly-evolving branches that feature in the hotspot models. Because the number of available gene sequences vary per species, the fastest branches may differ for a particular gene. The key shows branches found in each hotspot model. In hotspot 1, branches found include: Strisores (consisting of nightjars and their allies, swifts and hummingbirds), Darwin's finches, and Phasianidae (represented by the red-jungle fowl). In hotspot 2, branches include: Darwin's finches, Phasianidae, Aptenodytes (represented by the emperor penguin) and Buceros (represented by the Rhinoceros hornbill). Hotspot 3 contains the same branches as hotspot 2

Supporting Tables

Supplementary Table S1

Table S1: **Known candidate genes associated with beak shape morphology and size**

Gene symbol	Gene name	Description
ALX1	ALX Homeobox 1	Implicated in Lamichhaney et al (2015) as principle gene in a major locus contributing to beak shape diversity across Darwin's finches
BMP2	Bone Morphogenetic Protein 2	Shown to correlate with beak size but not shape (Abzhanov et al, 2004).
BMP4	Bone Morphogenetic Protein 4	Shown to correlate strongly with deep and broad beak morphology (Abzhanov et al, 2004).
BMP7	Bone Morphogenetic Protein 7	Shown to correlate with beak size but not shape (Abzhanov et al, 2004).
CALM1	Calmodulin 1	Shown to correlate with thin, elongated beak morphologies (Abzhanov et al, 2006).
COL4A5	Collagen Type IV Alpha 5 Chain	Shown to influence beak shape in great tits (Parus major) (Bosse et al., 2018)
DKK3	Dickkopf WNT Signaling Pathway Inhibitor 3	Incidicated to influence different beak shapes in Darwin's finches through expression variation (Mallarino et al., 2011)
DLK1	Delta Like Non-Canonical Notch Ligand 1	Shown in Chaves et al (2016) to correlate with beak size in Darwin's finches.
FOXC1	Forkhead Box C1	In the largest Fst value regions between Darwin's Finches with different beak sizes (Lamichhaney et al 2015).
GSC	Goosecoid Homeobox	In the largest Fst value regions between Darwin's Finches with different beak sizes (Lamichhaney et al 2015).
HMGA2	High Mobility Group AT-Hook 2	Implicated in Lamichhaney et al (2016) to influence beak size in species of Darwin's finches and in Chaves et al (2016).
LEMD3	LEM Domain Containing 3	Part of a locus with significant influence on beak size In Darwin's finches (Lamichhaney et al 2016)
LRRIQ1	Leucine Rich Repeats And IQ Motif Containing 1	Part of a locus with significant influence on beak size In Darwin's finches (Lamichhaney et al 2016)
MSRB3	Methionine Sulfoxide Reductase B3	Part of a locus with significant influence on beak size In Darwin's finches (Lamichhaney et al 2016)
RDH14	Retinol Dehydrogenase 14	In the largest Fst value regions between Darwin's Finches with different beak sizes (Lamichhaney et al 2015).
TGFBR2	Transforming Growth Factor Beta Receptor 2	Incidicated to influence different beak shapes in Darwin's finches through expression variation (Mallarino et al., 2011)
WIF1	WNT Inhibitory Factor 1	Part of a locus with significant influence on beak size In Darwin's finches (Lamichhaney et al 2016)
IGF1	Insulin-like growth factor 1	Associated with bill size in Pyrenestes ostrinus (Vonholdt et al., 2018)

Supplementary Table S2

Table S2: **Species names and file locations used for the whole genome alignment.**

Species name full	Coding analysis	ASCHE analysis	Location (ftp://ftp.ncbi.nlm.nih.gov/genomes/all/GCA) and version
Acanthisitta chloris	x	x	/000/695/815/GCA_000695815.1_ASM69581v1/GCA_000695815.1_ASM69581v1_genomic.fna.gz
Amazona aestiva		x	/001/420/675/GCA_001420675.1_ASM142067v1/GCA_001420675.1_ASM142067v1_genomic.fna.gz
Amazona vittata		x	/000/332/375/GCA_000332375.1_AV1/GCA_000332375.1_AV1_genomic.fna.gz
Anas platyrhynchos	x	x	/000/355/885/GCA_000355885.1_BGI_duck_1.0/GCA_000355885.1_BGI_duck_1.0_genomic.fna.gz
Anser cygnoides domesticus	x	x	/000/971/095/GCA_000971095.1_AnsCyg_PRJNA183603_v1.0/GCA_000971095.1_AnsCyg_PRJNA183603_v1.0_genomic.fna.gz
Apaloderma vittatum	x	x	/000/703/405/GCA_000703405.1_ASM70340v1/GCA_000703405.1_ASM70340v1_genomic.fna.gz
Aptenodytes forsteri	x	x	/000/699/145/GCA_000699145.1_ASM69914v1/GCA_000699145.1_ASM69914v1_genomic.fna.gz
Apteryx australis mantelli	x	x	/001/039/765/GCA_001039765.2_AptMant0/GCA_001039765.2_AptMant0_genomic.fna.gz
Aquila chrysaetos canadensis	x	x	/000/766/835/GCA_000766835.1_Aquila_chrysaetos-1.0.2/GCA_000766835.1_Aquila_chrysaetos-1.0.2_genomic.fna.gz
Ara macao		x	/000/400/695/GCA_000400695.1_SMACv1.1/GCA_000400695.1_SMACv1.1_genomic.fna.gz
Balearica regulorum gibbericeps	x	x	/000/709/895/GCA_000709895.1_ASM70989v1/GCA_000709895.1_ASM70989v1_genomic.fna.gz
Buceros rhinoceros silvestris	x	x	/000/710/305/GCA_000710305.1_ASM71030v1/GCA_000710305.1_ASM71030v1_genomic.fna.gz
Calidris pugnax	x	x	/001/431/845/GCA_001431845.1_ASM143184v1/GCA_001431845.1_ASM143184v1_genomic.fna.gz
Calypte anna	x	x	/000/699/085/GCA_000699085.1_ASM69908v1/GCA_000699085.1_ASM69908v1_genomic.fna.gz
Caprimulgus carolinensis	x	x	/000/700/745/GCA_000700745.1_ASM70074v1/GCA_000700745.1_ASM70074v1_genomic.fna.gz
Cariama cristata	x	x	/000/690/535/GCA_000690535.1_ASM69053v1/GCA_000690535.1_ASM69053v1_genomic.fna.gz
Cathartes aura		x	/000/699/945/GCA_000699945.1_ASM69994v1/GCA_000699945.1_ASM69994v1_genomic.fna.gz
Chaetura pelagica	x	x	/000/747/805/GCA_000747805.1_ChaPel_1.0/GCA_000747805.1_ChaPel_1.0_genomic.fna.gz
Charadrius vociferus	x	x	/000/708/025/GCA_000708025.2_ASM70802v2/GCA_000708025.2_ASM70802v2_genomic.fna.gz
Chlamydotis macqueenii	x	x	/000/695/195/GCA_000695195.1_ASM69519v1/GCA_000695195.1_ASM69519v1_genomic.fna.gz
Colinus virginianus		x	/000/599/465/GCA_000599465.1_NB1.1/GCA_000599465.1_NB1.1_genomic.fna.gz
Colius striatus	x	x	/000/690/715/GCA_000690715.1_ASM69071v1/GCA_000690715.1_ASM69071v1_genomic.fna.gz
Columba livia	x	x	/001/887/795/GCA_001887795.1_colLiv2/GCA_001887795.1_colLiv2_genomic.fna.gz
Corvus brachyrhynchos	x	x	/000/691/975/GCA_000691975.1_ASM69197v1/GCA_000691975.1_ASM69197v1_genomic.fna.gz
Corvus cornix cornix	x	x	/000/738/735/GCA_000738735.1_Hooded_Crow_genome/GCA_000738735.1_Hooded_Crow_genome_genomic.fna.gz
Coturnix japonica	x	x	/000/511/605/GCA_000511605.2_Coja_2.0a/GCA_000511605.2_Coja_2.0a_genomic.fna.gz
Cuculus canorus	x	x	/000/709/325/GCA_000709325.1_ASM70932v1/GCA_000709325.1_ASM70932v1_genomic.fna.gz
Egretta garzetta	x	x	/000/687/185/GCA_000687185.1_ASM68718v1/GCA_000687185.1_ASM68718v1_genomic.fna.gz
Eurypyga helias	x	x	/000/690/775/GCA_000690775.1_ASM69077v1/GCA_000690775.1_ASM69077v1_genomic.fna.gz
Falco cherrug	x	x	/000/337/975/GCA_000337975.1_F_cherrug_v1.0/GCA_000337975.1_F_cherrug_v1.0_genomic.fna.gz
Falco peregrinus	x	x	/001/887/755/GCA_001887755.1_falPer2/GCA_001887755.1_falPer2_genomic.fna.gz
Ficedula albicollis	x	x	/000/247/815/GCA_000247815.2_FicAlb1.5/GCA_000247815.2_FicAlb1.5_genomic.fna.gz
Fulmarus glacialis	x	x	/000/690/835/GCA_000690835.1_ASM69083v1/GCA_000690835.1_ASM69083v1_genomic.fna.gz
Gallus gallus	x	x	/000/002/315/GCA_000002315.3_Gallus_gallus-5.0/GCA_000002315.3_Gallus_gallus-5.0_genomic.fna.gz
Gavia stellata	x	x	/000/690/875/GCA_000690875.1_ASM69087v1/GCA_000690875.1_ASM69087v1_genomic.fna.gz
Geospiza fortis	x	x	/000/277/835/GCA_000277835.1_GeoFor_1.0/GCA_000277835.1_GeoFor_1.0_genomic.fna.gz
Haliaeetus albicilla	x	x	/000/691/405/GCA_000691405.1_ASM69140v1/GCA_000691405.1_ASM69140v1_genomic.fna.gz
Haliaeetus leucocephalus	x	x	/000/737/465/GCA_000737465.1_Haliaeetus_leucocephalus-4.0/GCA_000737465.1_Haliaeetus_leucocephalus-4.0_genomic.fna.gz
Lepidothrix coronata		x	/001/604/755/GCA_001604755.1_Lepidothrix_coronata-1.0/GCA_001604755.1_Lepidothrix_coronata-1.0_genomic.fna.gz
Leptosomus discolor	x	x	/000/691/785/GCA_000691785.1_ASM69178v1/GCA_000691785.1_ASM69178v1_genomic.fna.gz
Lyrurus tetrix tetrix		x	/000/586/395/GCA_000586395.1_tetTet1/GCA_000586395.1_tetTet1_genomic.fna.gz
Manacus vitellinus	x	x	/000/692/015/GCA_000692015.2_ASM69201v2/GCA_000692015.2_ASM69201v2_genomic.fna.gz
Meleagris gallopavo	x	x	/000/146/605/GCA_000146605.3_Turkey_5.0/GCA_000146605.3_Turkey_5.0_genomic.fna.gz
Melopsittacus undulatus	x	x	/000/238/935/GCA_000238935.1_Melopsittacus_undulatus_6.3/GCA_000238935.1_Melopsittacus_undulatus_6.3_genomic.fna.gz
Merops nubicus	x	x	/000/691/845/GCA_000691845.1_ASM69184v1/GCA_000691845.1_ASM69184v1_genomic.fna.gz
Mesitornis unicolor	x	x	/000/695/765/GCA_000695765.1_ASM69576v1/GCA_000695765.1_ASM69576v1_genomic.fna.gz
Nestor notabilis	x	x	/000/696/875/GCA_000696875.1_ASM69687v1/GCA_000696875.1_ASM69687v1_genomic.fna.gz
Nipponia nippon	x	x	/000/708/225/GCA_000708225.1_ASM70822v1/GCA_000708225.1_ASM70822v1_genomic.fna.gz
Opisthocomus hoazin	x	x	/000/692/075/GCA_000692075.1_ASM69207v1/GCA_000692075.1_ASM69207v1_genomic.fna.gz
Parus major	x	x	/001/522/545/GCA_001522545.2_Parus_major1.1/GCA_001522545.2_Parus_major1.1_genomic.fna.gz
Passer domesticus		x	/001/700/915/GCA_001700915.1_Passer_domesticus-1.0/GCA_001700915.1_Passer_domesticus-1.0_genomic.fna.gz
Pelecanus crispus	x	x	/000/687/375/GCA_000687375.1_ASM68737v1/GCA_000687375.1_ASM68737v1_genomic.fna.gz
Phaethon lepturus	x	x	/000/687/285/GCA_000687285.1_ASM68728v1/GCA_000687285.1_ASM68728v1_genomic.fna.gz

Table S2: **Species names and file locations used for the whole genome alignment.** *(continued)*

Species name full	Coding analysis	ASCHE analysis	Location (ftp://ftp.ncbi.nlm.nih.gov/genomes/all/GCA) and version
Phalacrocorax carbo	x	x	/000/708/925/GCA_000708925.1_ASM70892v1/GCA_000708925.1_ASM70892v1_genomic.fna.gz
Phoenicopterus ruber ruber		x	/000/687/265/GCA_000687265.1_ASM68726v1/GCA_000687265.1_ASM68726v1_genomic.fna.gz
Phylloscopus plumbeitarsus		x	/001/655/115/GCA_001655115.1_GWplu1.0/GCA_001655115.1_GWplu1.0_genomic.fna.gz
Picoides pubescens	x	x	/000/699/005/GCA_000699005.1_ASM69900v1/GCA_000699005.1_ASM69900v1_genomic.fna.gz
Podiceps cristatus		x	/000/699/545/GCA_000699545.1_ASM69954v1/GCA_000699545.1_ASM69954v1_genomic.fna.gz
Pseudopodoces humilis	x	x	/000/331/425/GCA_000331425.1_PseHum1.0/GCA_000331425.1_PseHum1.0_genomic.fna.gz
Pterocles gutturalis	x	x	/000/699/245/GCA_000699245.1_ASM69924v1/GCA_000699245.1_ASM69924v1_genomic.fna.gz
Pygoscelis adeliae	x	x	/000/699/105/GCA_000699105.1_ASM69910v1/GCA_000699105.1_ASM69910v1_genomic.fna.gz
Serinus canaria	x	x	/000/534/875/GCA_000534875.1_SCA1/GCA_000534875.1_SCA1_genomic.fna.gz
Setophaga coronata coronata		x	/001/746/935/GCA_001746935.1_mywagenomev1.1/GCA_001746935.1_mywagenomev1.1_genomic.fna.gz
Struthio camelus australis	x	x	/000/698/965/GCA_000698965.1_ASM69896v1/GCA_000698965.1_ASM69896v1_genomic.fna.gz
Sturnus vulgaris	x	x	/001/447/265/GCA_001447265.1_Sturnus_vulgaris-1.0/GCA_001447265.1_Sturnus_vulgaris-1.0_genomic.fna.gz
Taeniopygia guttata	x	x	/000/151/805/GCA_000151805.2_Taeniopygia_guttata-3.2.4/GCA_000151805.2_Taeniopygia_guttata-3.2.4_genomic.fna.gz
Tauraco erythrolophus	x	x	/000/709/365/GCA_000709365.1_ASM70936v1/GCA_000709365.1_ASM70936v1_genomic.fna.gz
Tinamus guttatus	x	x	/000/705/375/GCA_000705375.2_ASM70537v2/GCA_000705375.2_ASM70537v2_genomic.fna.gz
Tympanuchus cupido pinnatus		x	/001/870/855/GCA_001870855.1_T_cupido_pinnatus_GPC_3440_v1/GCA_001870855.1_T_cupido_pinnatus_GPC_3440_v1_genomic.fna.gz
Tyto alba		x	/000/687/205/GCA_000687205.1_ASM68720v1/GCA_000687205.1_ASM68720v1_genomic.fna.gz
Zonotrichia albicollis	x	x	/000/385/455/GCA_000385455.1_Zonotrichia_albicollis-1.0.1/GCA_000385455.1_Zonotrichia_albicollis-1.0.1_genomic.fna.gz
Zosterops lateralis melanops		x	/001/281/735/GCA_001281735.1_ASM128173v1/GCA_001281735.1_ASM128173v1_genomic.fna.gz

Supplementary Table S3

Table S3: **Top 20 identified motifs from 39,806 genomic regions** that show significant substitution rate variation in a phylogeny-based approach were branches were binned according their beak shape morphological rate. The canonical sequences of the 20 motifs are listed along with the number of predictions from the genomic regions, the respective sequence logos and the top 5 GO predictions.

Motif	Logo	Predictions	Top 5 specific predictions
AAAYR		63	MF olfactory receptor activity BP sensory perception of smell BP G-protein coupled receptor protein signaling pathway BP calcium-dependent cell-cell adhesion MF taste receptor activity
ACGT		373	MF RNA binding BP nuclear mRNA splicing, via spliceosome CC spliceosomal complex BP rRNA processing BP cell division
ACRG		219	BP G-protein coupled receptor protein signaling pathway MF serine-type endopeptidase activity BP defense response to bacterium MF hormone activity MF serine-type endopeptidase inhibitor activity
AWTAAW		15	MF olfactory receptor activity BP sensory perception of smell BP G-protein coupled receptor protein signaling pathway BP response to stimulus BP gene expression
AWTTAC		15	MF olfactory receptor activity BP sensory perception of smell BP G-protein coupled receptor protein signaling pathway BP inflammatory response MF eukaryotic cell surface binding
BCCATTA		13	MF olfactory receptor activity BP sensory perception of smell BP G-protein coupled receptor protein signaling pathway BP response to stimulus MF motor activity
CACG		438	BP rRNA processing MF ATP binding BP DNA repair MF translation regulator activity BP protein folding
CAG		631	MF calcium ion binding MF serine-type endopeptidase activity CC keratin filament MF potassium ion binding BP excretion
CAKCTGB		58	CC extracellular space BP muscle contraction CC proteinaceous extracellular matrix MF calcium ion binding CC Z disc
CATAAAHC		18	MF olfactory receptor activity BP sensory perception of smell BP G-protein coupled receptor protein signaling pathway BP defense response BP immune response
CTBCC		765	MF potassium ion binding BP potassium ion transport MF protein homodimerization activity MF growth factor activity MF extracellular matrix structural constituent
CTBCWG		424	CC extracellular space CC proteinaceous extracellular matrix MF calcium ion binding CC keratin filament MF sugar binding
CTCCTMC		394	BP transmembrane receptor protein tyrosine kinase signaling pathway BP anterior/posterior pattern formation BP lung development BP gland development MF SH3 domain binding
CTGKVA		125	MF serine-type endopeptidase activity BP excretion CC keratin filament BP innate immune response BP regulation of production of small RNA involved in gene silencing by RNA
DAAWTA		19	MF olfactory receptor activity BP sensory perception of smell BP G-protein coupled receptor protein signaling pathway BP defense response CC ER to Golgi transport vesicle
GGGATTW		17	MF olfactory receptor activity BP sensory perception of smell BP phototransduction BP nucleobase, nucleoside, nucleotide and nucleic acid metabolic process BP translation
GTGGGTGK		456	CC integral to plasma membrane BP muscle contraction MF sequence-specific DNA binding CC receptor complex MF transcription factor activity
MCATATGK		56	MF olfactory receptor activity BP sensory perception of smell BP G-protein coupled receptor protein signaling pathway BP defense response to bacterium MF serine-type endopeptidase inhibitor activity
TTYCCW		197	MF olfactory receptor activity BP sensory perception of smell BP G-protein coupled receptor protein signaling pathway CC extracellular space BP signal transduction
WAAYGW		44	MF olfactory receptor activity BP sensory perception of smell BP G-protein coupled receptor protein signaling pathway MF taste receptor activity BP defense response to bacterium

Supplemental References

Afanasyeva A, Bockwoldt M, Cooney CR, Heiland I, Gossmann TI. 2018. Human long intrinsically disordered protein regions are frequent targets of positive selection. *Genome research* **28**: 975–982. http://www.ncbi.nlm.nih.gov/pubmed/29858274 http://www.pubmedcentral.nih.gov/articlerender.fcgi?artid=PMC6028134.

Bailey TL. 2011. DREME: motif discovery in transcription factor ChIP-seq data. *Bioinformatics* **27**: 1653–1659. https://academic.oup.com/bioinformatics/article-lookup/doi/10.1093/bioinformatics/btr261.

Benjamini Y, Hochberg Y. 1995. Controlling the false discovery rate: a practical and powerful approach to multiple testing. *Journal of the Royal Statistical Society Series B (Methodological)*.

Brunskill EW, Potter AS, Distasio A, Dexheimer P, Plassard A, Aronow BJ, Potter SS. 2014. A gene expression atlas of early craniofacial development. *Developmental biology* **391**: 133–46.

Cooney CR, Bright JA, Capp EJR, Chira AM, Hughes EC, Moody CJA, Nouri LO, Varley ZK, Thomas GH. 2017. Mega-evolutionary dynamics of the adaptive radiation of birds. *Nature* **542**: 344–347. http://www.nature.com/doifinder/10.1038/nature21074.

Fletcher W, Yang Z. 2009. INDELible: A Flexible Simulator of Biological Sequence Evolution. *Molecular Biology and Evolution* **26**: 1879–1888. https://academic.oup.com/mbe/article-lookup/doi/10.1093/molbev/msp098.

Gupta S, Stamatoyannopoulos JA, Bailey TL, Noble W. 2007. Quantifying similarity between motifs. *Genome Biology* **8**: R24. http://genomebiology.biomedcentral.com/articles/10.1186/gb-2007-8-2-r24.

Hackett SJ, Kimball RT, Reddy S, Bowie RCK, Braun EL, Braun MJ, Chojnowski JL, Cox WA, Han K-L, Harshman J, et al. 2008. A Phylogenomic Study of Birds Reveals Their Evolutionary History. *Science* **320**: 1763–1768. http://www.sciencemag.org/cgi/doi/10.1126/science.1157704.

Hillier LW, Miller W, Birney E, Warren W, Hardison RC, Ponting CP, Bork P, Burt DW, Groenen MAM, Delany ME, et al. 2004. Sequence and comparative analysis of the chicken genome provide unique perspectives on vertebrate evolution. *Nature* **432**: 695–716. http://www.nature.com/doifinder/10.1038/nature03154.

Li L, Stoeckert CJJ, Roos DS. 2003. OrthoMCL: Identification of Ortholog Groups for Eukaryotic Genomes. *Genome Research* **13**: 2178–2189. http://genome.cshlp.org/cgi/content/full/13/9/2178.

Lloyd SP. 1982. Least Squares Quantization in PCM. *IEEE Transactions on Information Theory*.

Löytynoja A, Goldman N. 2008. Phylogeny-aware gap placement prevents errors in sequence alignment and evolutionary analysis. *Science* **320**: 1632–1635.

O'Leary NA, Wright MW, Brister JR, Ciufo S, Haddad D, McVeigh R, Rajput B, Robbertse B, Smith-White B, Ako-Adjei D, et al. 2016. Reference sequence (RefSeq) database at NCBI: current status, taxonomic expansion, and functional annotation. *Nucleic Acids Research* **44**: D733–D745. https://academic.oup.com/nar/article-lookup/doi/10.1093/nar/gkv1189.

Östlund G, Schmitt T, Forslund K, Köstler T, Messina DN, Roopra S, Frings O, Sonnhammer EL. 2009. Inparanoid 7: New algorithms and tools for eukaryotic orthology analysis. *Nucleic Acids Research* **38**: 196–203.

Prum RO, Berv JS, Dornburg A, Field DJ, Townsend JP, Lemmon EM, Lemmon AR. 2015. A comprehensive phylogeny of birds (Aves) using targeted next-generation DNA sequencing. *Nature* **526**: 569–573. http://www.nature.com/doifinder/10.1038/nature15697.

R Core Team. 2018. *R: A Language and Environment for Statistical Computing*. R Foundation for Statistical Computing, Vienna, Austria https://www.r-project.org/.

Revell LJ. 2012. phytools: An R package for phylogenetic comparative biology (and other things). *Methods in Ecology and Evolution*.

Suyama M, Torrents D, Bork P. 2006. PAL2NAL: Robust conversion of protein sequence alignments into the corresponding codon alignments. *Nucleic Acids Research* **34**: 609–612.

Szklarczyk D, Franceschini A, Wyder S, Forslund K, Heller D, Huerta-Cepas J, Simonovic M, Roth A, Santos A, Tsafou KP, et al. 2015. STRING v10: Protein-protein interaction networks, integrated over the tree of life. *Nucleic Acids Research* **43**: D447–D452.

Talavera G, Castresana J. 2007. Improvement of phylogenies after removing divergent and ambiguously aligned blocks from protein sequence alignments. *Systematic Biology* **56**: 564–577.

Venditti C, Meade A, Pagel M. 2011. Multiple routes to mammalian diversity. *Nature* **479**: 393–396. http://dx.doi.org/10.1038/nature10516.

Wang J, Vasaikar S, Shi Z, Greer M, Zhang B. 2017. WebGestalt 2017: a more comprehensive, powerful, flexible and interactive gene set enrichment analysis toolkit. *Nucleic Acids Research* **45**: W130–W137. https://academic.oup.com/nar/article-lookup/doi/10.1093/nar/gkx356.

Warren WC, Hillier LW, Tomlinson C, Minx P, Kremitzki M, Graves T, Markovic C, Bouk N, Pruitt KD, Thibaud-Nissen F, et al. 2017. A New Chicken Genome Assembly Provides Insight into Avian Genome Structure. *G3 Genes|Genomes|Genetics* **7**: 109–117. http://g3journal.org/lookup/doi/10.1534/g3.116.035923.

Wilkinson L. 2011. ggplot2: Elegant Graphics for Data Analysis by WICKHAM, H. *Biometrics*.

Wu M, Chatterji S, Eisen JA. 2012. Accounting for alignment uncertainty in phylogenomics. *PLoS ONE* **7**: 1–10.

Yang Z. 1998. Likelihood ratio tests for detecting positive selection and application to primate lysozyme evolution. *Molecular Biology and Evolution* **15**: 568–573. https://academic.oup.com/mbe/article-lookup/doi/10.1093/oxfordjournals.molbev.a025957.

Yang Z. 2007. PAML 4: Phylogenetic analysis by maximum likelihood. *Molecular Biology and Evolution* **24**: 1586–1591.

Yang Z, Nielsen R, Hasegawa M. 1998. Models of Amino Acid Substitution and Applications to Mitochondrial Protein Evolution. *Mol Biol Evol* **15**: 1600–1611.

Zhang G, Li C, Li Q, Li B, Larkin DM, Lee C, Storz JF, Antunes A, Greenwold MJ, Meredith RW, et al. 2014. Comparative genomics reveals insights into avian genome evolution and adaptation. *Science* **346**: 1311–1320. http://www.sciencemag.org/cgi/doi/10.1126/science.1251385.